NASA
Technical Paper 1926

AVRADCOM
Technical Report 81-B-5

AD A108790

Wind-Tunnel Investigation of the Effects of Blade Tip Geometry on the Interaction of Torsional Loads and Performance for an Articulated Helicopter Rotor

William T. Yeager, Jr., and Wayne R. Mantay

DECEMBER 1981

NASA

81 12 22 054

NASA
Technical Paper 1926

AVRADCOM
Technical Report 81-B-5

Wind-Tunnel Investigation of the Effects of Blade Tip Geometry on the Interaction of Torsional Loads and Performance for an Articulated Helicopter Rotor

William T. Yeager, Jr., and Wayne R. Mantay
Structures Laboratory
AVRADCOM Research and Technology Laboratories
Langley Research Center
Hampton, Virginia

SUMMARY

An investigation was conducted in the Langley Transonic Dynamics Tunnel to determine the effects of rotor blade tip geometry on the interaction between torsional loads and performance for an articulated helicopter rotor. Tests were conducted on four tip geometries at advance ratios of 0.20, 0.30, and 0.35. Geometric variations between tips consisted of taper, sweep, and anhedral. Results indicate that for the configurations tested, there is not a strong correlation between blade torsional loads and rotor performance. Alleviation of torque requirements on the advancing side of the rotor was found to be more important to rotor performance than reduction of torque requirements on the retreating side. Analyses show that the rotor inflow model used is an important parameter in rotor performance prediction. Neither rigid-blade solidity effects, inflow environment, nor blade torsional loads can be used independently to accurately predict adaptive rotor performance.

INTRODUCTION

During high-speed helicopter flight, rotor operating limits essentially result from unfavorable spanwise and azimuthal air-load distributions. As the forward speed of the helicopter increases, the rotor disk is asymmetrically loaded because of differences in relative velocity encountered around the azimuth by the blades. Blade sections on the advancing side of the disk may experience compressibility effects, and/or blade sections on the retreating side of the disk may encounter stall effects. To increase forward flight efficiency while maintaining hover efficiency, designers have built in blade twist, used advanced airfoil sections, and changed solidity to improve overall rotor air-load distribution. These efforts have resulted in compromises that affect hover and forward flight performance. For example, the large amounts of static twist applied for hover efficiency can result in limitations on forward flight, such as high flapwise stresses on blades (ref. 1).

To avoid fixed-geometry blade restrictions, conformable rotor concepts have been considered (refs. 1 to 4). These passive rotor designs, by allowing the blade to adapt to an operating condition by means of favorable dynamic twist, would improve performance and reduce vibratory blade loads. One method of providing and tailoring blade dynamic twist is by changing the blade tip geometry (refs. 3 and 4). To be effective, this dynamic twist should produce a nose-up blade twist component in high-speed forward flight. This nose-up dynamic twist allows larger values of nose-down static twist to be built into the blade to improve hover efficiency. Reducing the nose-down twist in forward flight might lessen compressibility effects on the advancing side ($\psi = 90°$) of the rotor as well as reduce the blade flapwise stresses. However, nose-down twist should not be reduced to a level that would introduce stall effects on the retreating side ($\psi = 270°$) of the rotor.

An investigation was conducted to determine the degree of correlation between rotor performance and the dynamic twist generated by changing blade tip geometry. Blade torsional loads were used as an indication of blade dynamic twist. Data for this investigation were obtained from a test conducted in the Langley Transonic Dynamics Tunnel on a 1/6-scale model helicopter rotor with four tip geometries.

Results of a rigid-blade analysis were correlated with experimental results in an attempt to isolate the effects of the aerodynamic environment and blade aeroelastic properties on rotor performance.

SYMBOLS

The positive directions of forces and angles are shown in figure 1.

a speed of sound

C_D rotor drag coefficient, $\dfrac{D}{\rho \pi R^2 (\Omega R)^2}$

C_L rotor lift coefficient, $\dfrac{L}{\rho \pi R^2 (\Omega R)^2}$

C_Q rotor torque coefficient, $\dfrac{Q}{\rho \pi R^3 (\Omega R)^2}$

D rotor drag, N

K_{θ_1} torsional deflection of strain-gaged station per unit torsional moment at that station, relative to next inboard strain-gaged station, positive nose-up, deg/N-m

L rotor lift, N

Q rotor shaft torque, N-m

R rotor radius, 137.16 cm

r spanwise distance along blade radius measured from center of rotation, cm

V free-stream velocity, m/sec

α angle of attack of rotor blade section, deg

α_s angle of attack of rotor shaft, deg

θ_1 twist angle built into rotor blade, positive nose-up, deg

μ rotor advance ratio, $\dfrac{V}{\Omega R}$

ρ mass density of test medium, kg/m^3

σ rotor solidity ratio, $\dfrac{\text{Total blade area}}{\text{Rotor disk area}}$

2

ψ	azimuth angle of rotor blade, deg
Ω	rotor rotational speed, rad/sec
ω	natural frequency of rotating blade, rad/sec

APPARATUS AND PROCEDURES

Wind Tunnel

The experimental program was conducted in the Langley Transonic Dynamics Tunnel (TDT) shown in figure 2. The TDT is a continuous flow tunnel with a slotted test section and is capable of operation up to Mach 1.2 at stagnation pressures up to 1 atm (101 kPa). The tunnel test section is 4.9 m square with cropped corners and has a cross-sectional area of 23 m^2. Either air or Freon-12[1] may be used as a test medium in the TDT. Because of its high density and low speed of sound, the use of Freon-12 aids the matching of full-scale Reynolds number and Mach number to model-scale values. Also, the restrictions on model structural design are eased, while dynamic similarity is still maintained. The heavier test medium permits a simplified structural design to obtain the required stiffness characteristics and thus eases the design and/or fabrication requirements of the model (ref. 5). For this investigation, Freon-12 at a nominal density of 3.09 kg/m^3 was used as the test medium.

Model Description

The rotor model used in this investigation was a 1/6-scale, four-blade articulated rotor with coincident lead-lag, and flapping hinges. The blade geometry and built-in twist distribution are shown in figure 3. The blades were designed so that tip configuration could be changed at the 91 percent radius. In addition to the baseline tip, three other tips (fig. 4) were studied which differed from the baseline tip in sweep angle, taper ratio, and anhedral. These tips are denoted as swept, tapered with and without anhedral, and double swept with anhedral. Incorporation of sweep angle in the tip geometries provides an offset of the tip aerodynamic center with respect to the inboard-blade elastic axis. Anhedral is used in an attempt to increase the vertical separation between a blade and the tip vortex shed by preceding blades (ref. 6). The blades geometrically represented a current full-scale utility-class rotor system. The blades were also aeroelastically scaled, but blade dynamic characteristics did not precisely represent any specific full-scale rotor. The blade physical properties, which are the same as those of the blades of reference 6, are presented in table I. An SC 1095 airfoil was used on the blades from the root cutout to 51 percent radius and from 84 percent radius to the tip. Between 51 and 84 percent radius, a cambered SC 1095-R8 airfoil was used. One blade was instrumented with four-arm strain-gage bridges to measure loads at several blade radial stations. Flapwise (out-of-plane) moments and chordwise (in-plane) moments were measured at 22, 40, 60, and 80 percent radius, while torsional moments were measured at 23, 41, and 81 percent radius.

The blades were tested on the aeroelastic rotor experimental system (ARES) shown in figures 5 and 6. The ARES has a generalized helicopter fuselage shape enclosing

---

[1]Freon: Registered trademark of E. I. du Pont de Nemours & Co., Inc.

the rotor controls and drive system. It is powered by a variable frequency synchronous motor rated at 35-kW output at 12 000 rpm. The motor is connected to the rotor shaft through a belt-driven two-stage speed reduction system. The ARES rotor control system and pitch attitude (α_s) are remotely controlled from within the wind-tunnel control room. The ARES pitch attitude is varied by an electrically controlled hydraulic actuator. Blade collective pitch and lateral and longitudinal cyclic pitch are input to the rotor through the swashplate. The swashplate is moved by three hydraulic actuators.

Instrumentation on the ARES allows continuous displays of model control settings, rotor forces and moments, blade loads, and pitch link loads. ARES pitch attitude is measured by an accelerometer, and rotor control positions are measured by linear potentiometers connected to the swashplate. Rotor blade flapping and lagging are measured by rotary potentiometers mounted on the rotor hub and geared to the blade cuff. Rotor shaft speed is determined by a magnetic sensor. The rotating blade data are transferred through a 30-channel slip-ring assembly. Rotor forces and moments are measured by a six-component strain-gage balance mounted below the pylon and drive system. The balance is fixed with respect to the rotor shaft and pitches with the fuselage. Fuselage forces and moments are not sensed by the balance.

Test Procedure

At each test point, the rotor rotational speed and tunnel conditions were adjusted to give the desired values of advancing tip Mach number and advance ratio. The model was then pitched to the desired shaft angle of attack. Blade collective pitch was changed to obtain a variation in rotor lift; and at each collective pitch setting, the cyclic pitch was used to remove rotor first-harmonic flapping with respect to the rotor shaft. Data were then recorded at each value of collective pitch. The maximum value of collective pitch attained at each shaft angle of attack was determined in most cases by either blade load limits or ARES drive system limits. Rotor aerodynamic performance and blade loads were measured at advance ratios of 0.20, 0.30, and 0.35 for shaft angles of attack from -2° to -12° and a rotational tip Mach number ($\Omega R/a$) of 0.61.

Model deadweight tares were determined throughout the shaft angle-of-attack range with the blades on and with them removed. Aerodynamic rotor hub tares were determined with the blades removed throughout the ranges of shaft angle of attack and advance ratio investigated. Both deadweight and hub aerodynamic tares have been removed from the data presented herein.

PRESENTATION OF RESULTS

The results in this report are presented in the figures as follows:

4

Based on approximately 160 repeated data points, the repeatability of the data for constant shaft angle of attack and advance ratio has been estimated to be within the following limits:

$$C_L/\sigma \pm 0.00200$$

$$C_D/\sigma \pm 0.00040$$

$$C_Q/\sigma \pm 0.00025$$

The value of σ used throughout this report for normalizing performance coefficients is 0.084, based on a blade nominal equivalent chord of 9.05 cm and a radius of 137.15 cm.

DISCUSSION OF RESULTS

As mentioned in the Introduction, the rotor operating environment should be improved by reducing nose-down twist on the advancing side of the rotor disk in forward flight while not introducing stall on the retreating side of the disk. To ensure that stall is not introduced on the retreating side, increased nose-down twist can be applied. To assess the correlation between measured blade torsional loads and rotor performance for each tip configuration, the criterion of reduced nose-down dynamic twist at $\psi = 90°$ (advancing side) and increased nose-down dynamic twist at $\psi = 270°$ (retreating side) is used in the following data discussion.

Experimental Results

Rotor performance.- The basic performance data for the four rotor configurations tested are presented in figures 7 to 10 as variations of C_L/σ with both C_D/σ and C_Q/σ for advance ratios μ of 0.20, 0.30, and 0.35. To facilitate comparisons between the four rotor configurations, cross plots of the data in figures 7 to 10 are presented in figure 11 as the variations of C_D/σ with C_Q/σ for different values of C_L/σ.

Comparison, where possible, between performance data presented herein and data of reference 6 (not shown in the figures) indicates a difference in the performance trends with advance ratio between the baseline tip and the swept, tapered tip with anhedral. This occurs only at low advance ratios. Differences in hub configurations and the resulting tares used in reference 6 for defining rotor task and resulting rotor angles may account for these performance trend differences, which do not affect the conclusions of this report. At the highest advance ratio, the two data sets agree in performance trends for these two tip configurations.

Rotor torsional loads.- Torsional moment data at r/R = 0.81 for each rotor tip configuration as a function of rotor azimuth are shown in figure 12 for selected values of C_T/σ and α_s at each test advance ratio. These selected conditions are representative of full-scale rotor force requirements at the advance ratios indicated. Although not presented, an analysis of the moment data for each rotor configuration indicated that the moment trends were essentially independent of shaft angle of attack for the rotor tasks of figure 12. The waveforms presented in figure 12 are formed from the first eight harmonics of a Fourier analysis of the strain-gage signal. As shown, the harmonic content of these waveforms is configuration dependent. Because the strain-gage location at r/R = 0.81 was farthest outboard, the torsional moment at that station was considered to be the most indicative of the tip contribution to blade dynamic twist. The azimuthal variations of the torsional moment at r/R = 0.23 and 0.41 show trends similar to the data at r/R = 0.81.

The radial distribution of mean torsional moment measured for each rotor tip configuration is shown in figure 13 for the same rotor tasks as in figure 12. The mean torsional moment at r/R = 0.81 was used as an indication of the mean dynamic twist provided by each tip configuration for the given rotor task.

The oscillatory ($\frac{1}{2}$ peak to peak) and mean torsional moment data contained herein agree with those of reference 6 in terms of configuration trends for tip shapes in common between the tests.

Correlation of blade torsional loads and rotor performance.- The correlation of blade torsional loads and rotor performance is shown in table II for the same nominal rotor tasks presented in figures 12 and 13. In table II, performance results are ranked in order of increasing C_Q/σ. The measured torsional loads at ψ = 90° and ψ = 270° are ranked in order of decreasing adherence to the following torsional loads criteria: at ψ = 90°, the configuration producing the most nose-up torsional moment is ranked first; while at ψ = 270°, the configuration producing the most nose-down torsional moment is ranked first. A correlation is shown between torsional moment and performance only at the lowest advance ratio, μ = 0.20, and only for ψ = 90°. Increasing the nose-down twist on the retreating side of the disk (ψ = 270°) did not correlate with performance improvements.

Also shown in table II is the degree of correlation between measured mean torsional load and forward flight performance. In table II, the tip producing the most nose-up mean torsional moment is ranked first, and the tip producing the least nose-up mean torsional moment is ranked last. Presentation of the mean torsional moment in this manner shows correlation with rotor performance at μ = 0.20 and 0.35, but not at μ = 0.30.

Several explanations can be offered for the results indicated in table II. The success of a passive conformable rotor depends on many aeroelastic parameters and their interactions. Reference 4 suggests that a swept tip could be used to produce dynamic nose-up twist on the advancing blade if a negative lift is produced on the tip. If the negative angle of attack on the advancing side of the rotor disk is not of the magnitude predicted by the uniform inflow analysis of reference 4, then the load on the tip may not be sufficient to untwist the blade. In fact, the negative angles of attack on the advancing side of the disk may not be of a magnitude to cause significant performance problems. Also, relief of the high angles of attack predicted on the retreating side of the disk by uniform inflow analysis (ref. 4) may not be a strong requirement for forward flight performance improvements. This can be shown by considering the correlation between the mean torsional loads and performance

6

presented in table II. The correlation between the mean torsional loads and performance is good when nose-up mean torsional loads are considered as the criterion for improved performance. Ranking of the mean torsional moments in the opposite manner in table II, i.e., least nose-up moment to most nose-up moment, would not show good correlation with rotor performance at any of the three test advance ratios; thus, alleviation of retreating-side torque requirements is secondary for performance improvements for these test conditions.

Analytical Results

Because of the results of the previous section, the authors felt that prediction of the performance of a passively conformable rotor and, ultimately, its design characteristics depend, to a large extent, on the inflow and resulting angle-of-attack environment experienced by the rotor. For this reason, the decision was made to analytically study the effect that both uniform and nonuniform inflow models might have on the correlation between measured rotor torsional loads and performance.

Rotor performance characteristics and azimuthal distributions of rotor-blade-section angle of attack were calculated with a computer program using a strip-theory implementation of the equations presented in reference 7. In the analysis, the blade was assumed to be rigid with pitch and flap degrees of freedom but no lag degree of freedom. The rotor airfoil section characteristics used were obtained from reference 8. Changes in section aerodynamic coefficients with angle of attack and Mach number were included in the analysis. All calculations were made by using both a uniform inflow model and the nonuniform inflow model from reference 9. Reference 9 considers a rotor load distribution which closely resembles that of a typical rotor and obtains an exact solution for the induced velocity at any point on the rotor. This model was largely confirmed by reference 10.

Angle-of-attack distributions.- The calculated angle of attack of the baseline blade tip (0.90 < r/R < 1.0) as a function of rotor azimuth is presented in figure 14 for μ = 0.20, 0.30, and 0.35 for the same rotor tasks as in figure 12.

The different angles of attack in the tip region predicted by the two inflow models would yield different tip lift distributions and thus different rotor performance and blade tip torsional responses. The angles of attack on the advancing side of the rotor disk predicted by the uniform inflow model may not be sufficiently negative to cause a swept tip blade of torsional stiffness tested herein to be twisted nose-up by the amount suggested for improved performance in reference 4. The angles of attack on the advancing side predicted by the nonuniform inflow model are generally more positive than those predicted by the uniform inflow model and indicate that use of an aft-swept tip could actually increase blade nose-down twist. Note that the torsional moment data presented in figure 12 are consistent with this conclusion and do indicate a positive lift acting on the tip, because the majority of the measured torsional loads at ψ = 90° are nose-down.

Performance.- The calculated rotor performance is presented in figure 15 for the baseline tip and the swept, tapered tip for advance ratios of 0.20, 0.30, and 0.35. The baseline and swept, tapered tip configurations were chosen for this analytical comparison because of their differing area solidities, 0.0843 and 0.0829, respectively. This solidity difference is, of course, due solely to changes in tip planform. The higher tip loading in a nonuniform inflow environment should result in different torque requirements for various tip planforms, whereas the uniform inflow analysis should not show as much evidence of tip solidity changes.

7

Comparison of analytical results (fig. 15) with experimental results (fig. 11) shows that the uniform inflow analysis (figs. 15(a) to 15(c)) predicts configuration performance trends similar to those observed experimentally only for $\mu = 0.20$. For $\mu = 0.30$, the analysis is marginal in predicting the experimental data trends, and for $\mu = 0.35$, the uniform inflow analysis fails to predict performance trends observed experimentally. The uniform inflow model consistently underpredicts the magnitude of rotor C_Q/σ for $\mu = 0.20$. As advance ratio increases to 0.30 and 0.35, the correlation between the uniform inflow theory and the magnitude of the experimental results improves, but this improvement is mainly at $C_L/\sigma = 0.04$ and 0.06.

The nonuniform inflow analysis predicts performance trends between tip configurations (figs. 15(d) to 15(f)) which for $\mu = 0.20$ and $\mu = 0.35$ are close to those shown by the wind-tunnel data in figure 11. For $\mu = 0.30$, the nonuniform inflow analysis fails to predict the performance trends between configurations (fig. 11(b)). The nonuniform inflow model shows good correlation between theory and test at $\mu = 0.20$ for $C_L/\sigma = 0.06$ and 0.08 with regard to the magnitude of rotor C_Q/σ. As advance ratio increases, the degree of C_Q/σ magnitude correlation is somewhat diminished but remains reasonable for $C_L/\sigma = 0.04$ and 0.06.

Both the trends and the magnitudes of the experimental rotor performance have been shown to be better predicted by the nonuniform inflow analysis than by the uniform inflow analysis. Because the nonuniform inflow analysis emphasizes tip load more than does the uniform inflow analysis, the predicted blade-section angles of attack presented in figure 14 for the nonuniform inflow analysis would appear to be representative of actual section angles of attack. Also note that the rigid-blade nonuniform inflow analysis failed to predict the performance trends of the selected rotor configurations at a condition ($\mu = 0.30$) for which the wind-tunnel data also show little correlation between blade torsional loads and rotor performance.

The prediction of performance trends between tip configurations discussed above is summarized in table III. From table III it appears that neither rigid-blade solidity effects, inflow environment, nor aeroelastic tailoring criteria can alone be used to totally predict performance trends found experimentally. However, a nonuniform inflow analysis incorporating solidity effects on a rigid blade appears to be the most successful in predicting rotor performance trends over the ranges of parameters investigated in this study.

8

CONCLUSIONS

An investigation has been conducted in the Langley Transonic Dynamics Tunnel to determine the degree of correlation between rotor performance and the dynamic twist generated by changes in blade tip geometry. Experimental studies were conducted on an articulated rotor with four different tip geometries at advance ratios of 0.20, 0.30, and 0.35. Calculated results for selected test configurations have been presented and compared with the experimental results. Calculated results were obtained by using uniform and nonuniform inflow models. Based on the data obtained, and for the test conditions and model configurations investigated, the following conclusions have been reached:

1. There does not appear to be a strong correlation between blade torsional loads and rotor performance prediction.

2. For a given rotor task at each advance ratio investigated, both the azimuthal variation of torsional moment and the mean torsional moment at 81 percent radius are configuration dependent.

3. Reducing the nose-down twist on the advancing blade appears to be more important to forward flight performance than increasing the nose-down twist on the retreating blade.

4. The rotor inflow model used is an important parameter in analytically predicting the performance of an adaptive rotor.

5. Neither rigid-blade solidity effects, inflow environment, nor blade torsional loads can be used alone to accurately predict adaptive rotor performance.

Langley Research Center
National Aeronautics and Space Administration
Hampton, VA 23665
September 28, 1981

REFERENCES

1. Lemnios, A. Z.; and Smith, A. F.: An Analytical Evaluation of the Controllable Twist Rotor Performance and Dynamic Behavior. USAAMRDL Tech. Rep. 72-16, U.S. Army, May 1972. (Available from DTIC as AD 747 808.)

2. Lemnios, A. Z.; Nettles, William E.; and Howes, H. E.: Full Scale Wind Tunnel Tests of a Controllable Twist Rotor. Proceedings of a Symposium on Rotor Technology, American Helicopter Soc., Aug. 1976.

3. Doman, Glidden S.; Tarzanin, Frank J.; and Shaw, John, Jr.: Investigation of Aeroelastically Adaptive Rotor Systems. Proceedings of a Symposium on Rotor Technology, American Helicopter Soc., Aug. 1976.

4. Blackwell, R. H.; and Merkley, D. J.: The Aeroelastically Conformable Rotor Concept. Preprint No. 78-59, American Helicopter Soc., May 1978.

5. Lee, Charles: Weight Considerations in Dynamically Similar Model Rotor Design. SAWE Paper No. 659, May 1968.

6. Weller, William H.: Experimental Investigation of Effects of Blade Tip Geometry on Loads and Performance for an Articulated Rotor System. NASA TP-1303, 1979.

7. Gessow, Alfred; and Crim, Almer D.: A Method for Studying the Transient Blade-Flapping Behavior of Lifting Rotors at Extreme Operating Conditions. NACA TN 3366, 1955.

8. Noonan, Kevin W.; and Bingham, Gene J.: Aerodynamic Characteristics of Three Helicopter Rotor Airfoil Sections at Reynolds Numbers From Model Scale to Full Scale at Mach Numbers From 0.35 to 0.90. NASA TP-1701, AVRADCOM TR 80-B-5, 1980.

9. Mangler K. W.; and Squire, H. B.: The Induced Velocity Field of a Rotor. R. & M. No. 2642, British A.R.C., May 1950.

10. Heyson, Harry H.; and Katzoff, S.: Induced Velocities Near a Lifting Rotor With Nonuniform Disk Loading. NACA Rep. 1319, 1957. (Supersedes NACA TN 3690 by Heyson and Katzoff and TN 3691 by Heyson.)

10

TABLE I.- MODEL ROTOR BLADE PROPERTIES

(a) Structural properties

Inboard station of segment, r/R	Segment length, m	Mass, kg	Structural stiffness, $N\text{-}m^2$			Radius of gyration of spar, m	K_{θ_1}, deg/N-m
			Chordwise	Flapwise	Torsional		
0.127	0.051	0.083	4611	174.1	168.7	0.000155	
.164	.027	.024	3366	107.4	122.5	.000155	
.184	.446	.475	1813	57.1	66.0	.000155	
a.230							0.269
a.410							.213
.508	.247	.254	1813	57.1	66.0	.000155	
.688	.206	.232	1813	57.1	66.0	.000155	
a.810							.472
.838	.067	.080	1813	57.1	66.0	.000155	
.887	.028	.015	2847	89.5	103.6	.000155	
.907	.042	.029	1813	57.1	66.0	.000155	
.938	.075	.028	1074	33.4	38.7	.000155	
.992	.009	.004	40	1.8	7.1	.000155	

[a] Blade stations instrumented for torsional moment.

(b) Model rotor blade rotating natural frequencies

ω/Ω	Mode identity
1.04	Flapwise
3.67	Flapwise
6.24	Flapwise
8.91	Chordwise
11.00	Torsional

TABLE II.- CORRELATION OF ROTOR PERFORMANCE WITH TORSIONAL LOADS FOR $C_L/\sigma = 0.08$

Numbers in table indicate ranking of each configuration with respect to performance (lowest C_Q/σ ranked first), torsional load at $\psi = 90°$ (most nose-up moment ranked first), torsional load at $\psi = 270°$ (most nose-down moment ranked first), and mean torsional load (most nose-up moment ranked first)

(a) $\mu = 0.20$, $\alpha_s = -4°$

Tip configuration	Rank with respect to -			
	Performance	Loads		
		$\psi = 90°$	$\psi = 270°$	Mean
Double-swept with anhedral	1	1	4	1
Baseline	2	3	3	2
Swept, tapered	3	2	1	3
Swept, tapered with anhedral	4	4	2	4

(b) $\mu = 0.30$, $\alpha_s = -4°$

Tip configuration	Rank with respect to -			
	Performance	Loads		
		$\psi = 90°$	$\psi = 270°$	Mean
Baseline	1	3	4	3
Swept, tapered	2	1	2	2
Swept, tapered with anhedral	3	4	1	4
Double-swept with anhedral	4	2	3	1

(c) $\mu = 0.35$, $\alpha_s = -6°$

Tip configuration	Rank with respect to -			
	Performance	Loads		
		$\psi = 90°$	$\psi = 270°$	Mean
Double-swept with anhedral	1	2	3	1
Baseline	2	3	4	3
Swept, tapered	3	1	2	2
Swept, tapered with anhedral	4	4	1	4

12

TABLE III.- PERFORMANCE PREDICTION FOR BASELINE AND SWEPT-TAPERED TIPS

μ	Rigid-blade, solidity effects, uniform inflow	Rigid-blade, solidity effects, nonuniform inflow	Aeroelastic tailoring (ref. 4), torsional load/performance correlation
0.2	Predicts	Predicts	Predicts
.3	Fails to predict	Fails to predict	Fails to predict
.35	Fails to predict	Predicts	Fails to predict
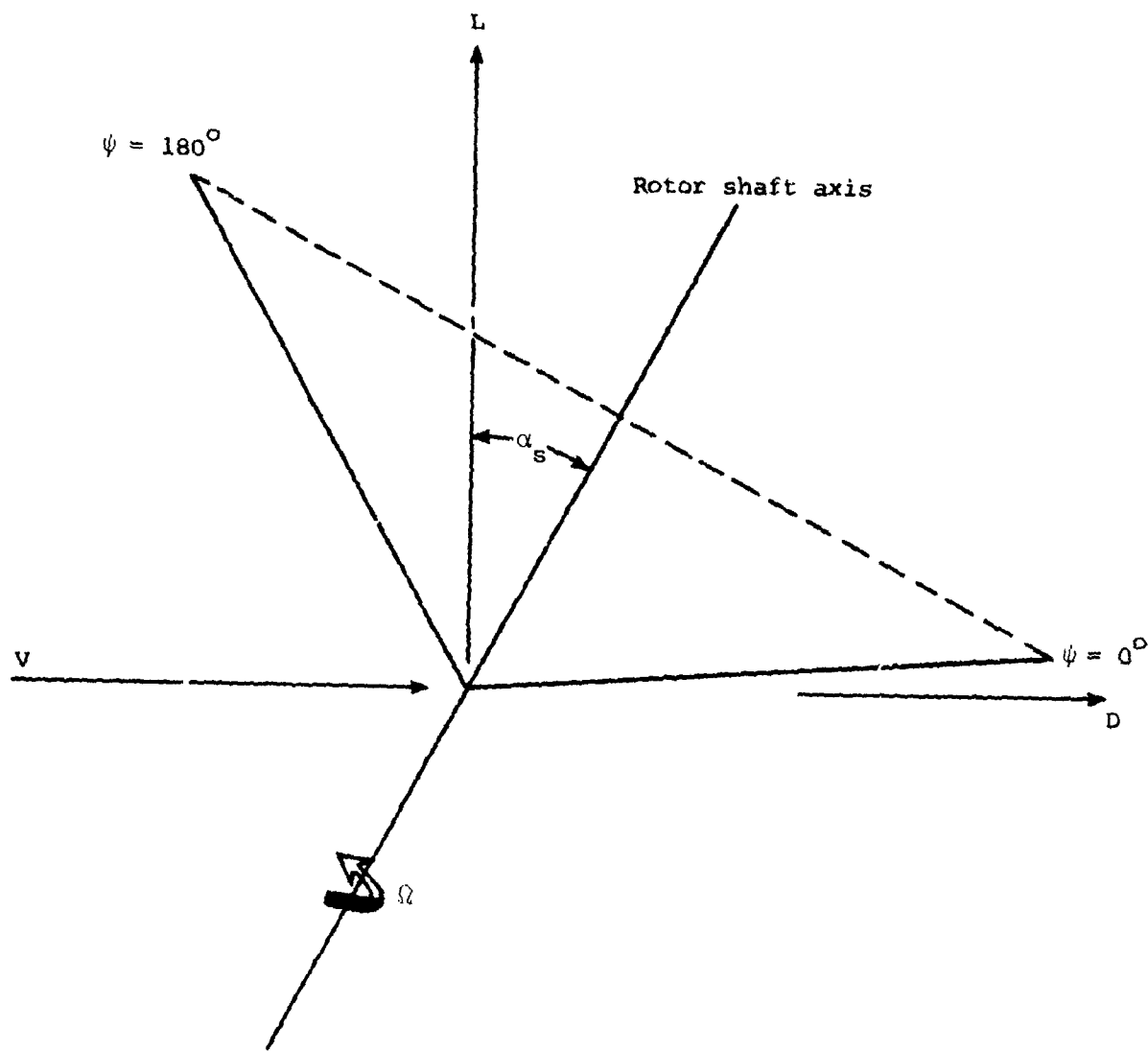
Figure 1.- Notation showing positive direction of forces, angles, and velocities.
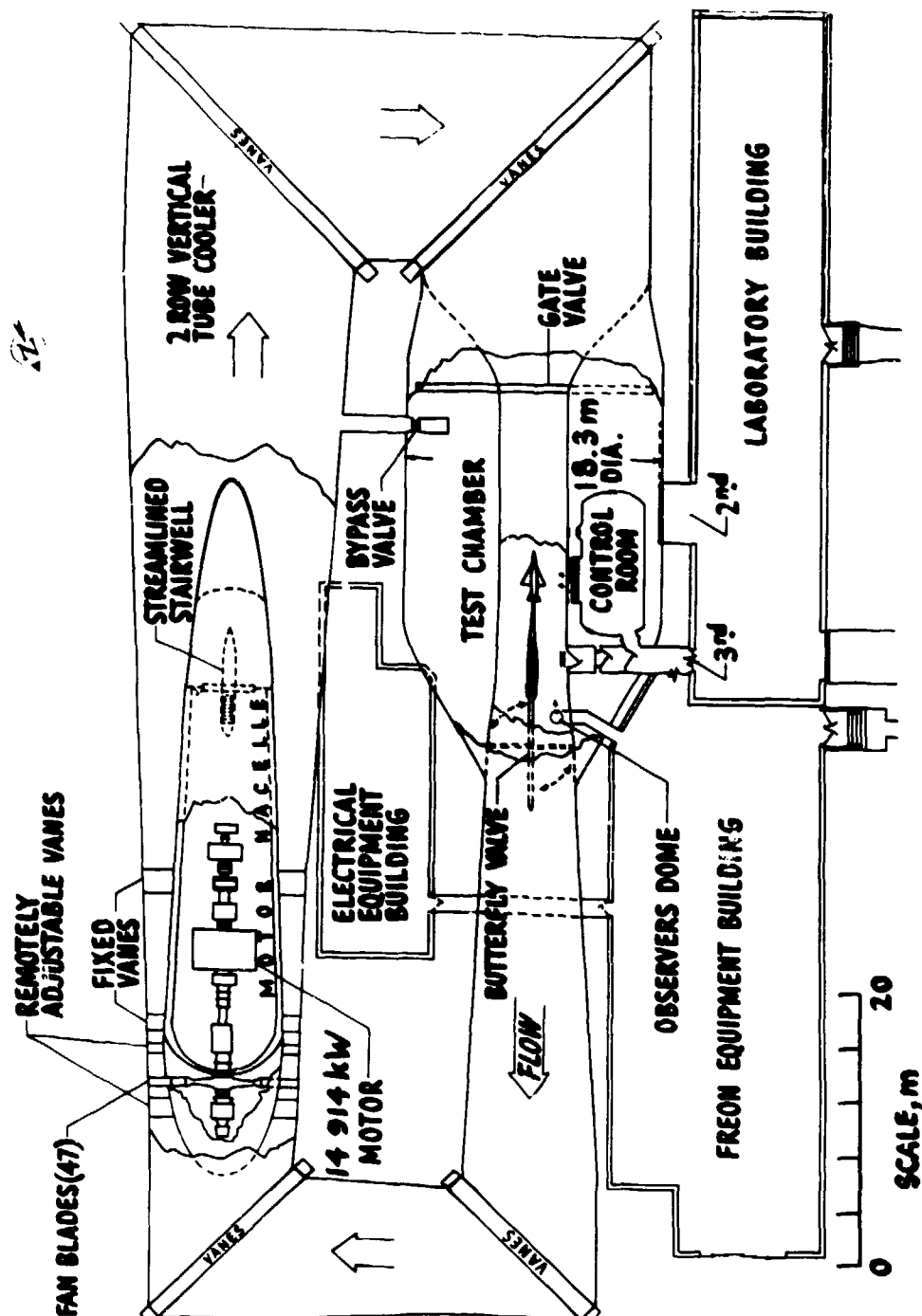
Figure 2.- Langley Transonic Dynamics Tunnel.

15

Figure 2. - Concluded.

16
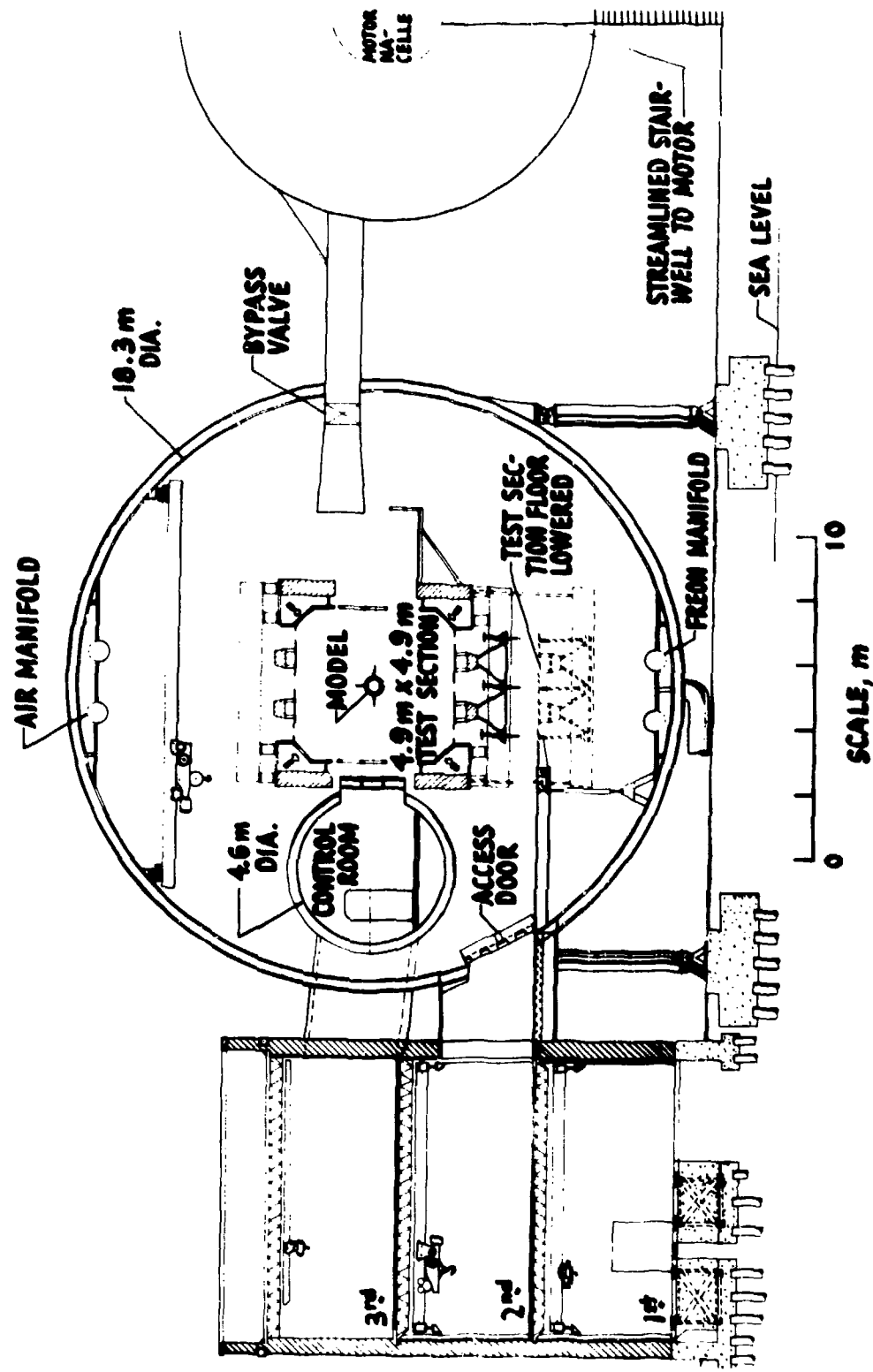
Dimensions are given in centimeters
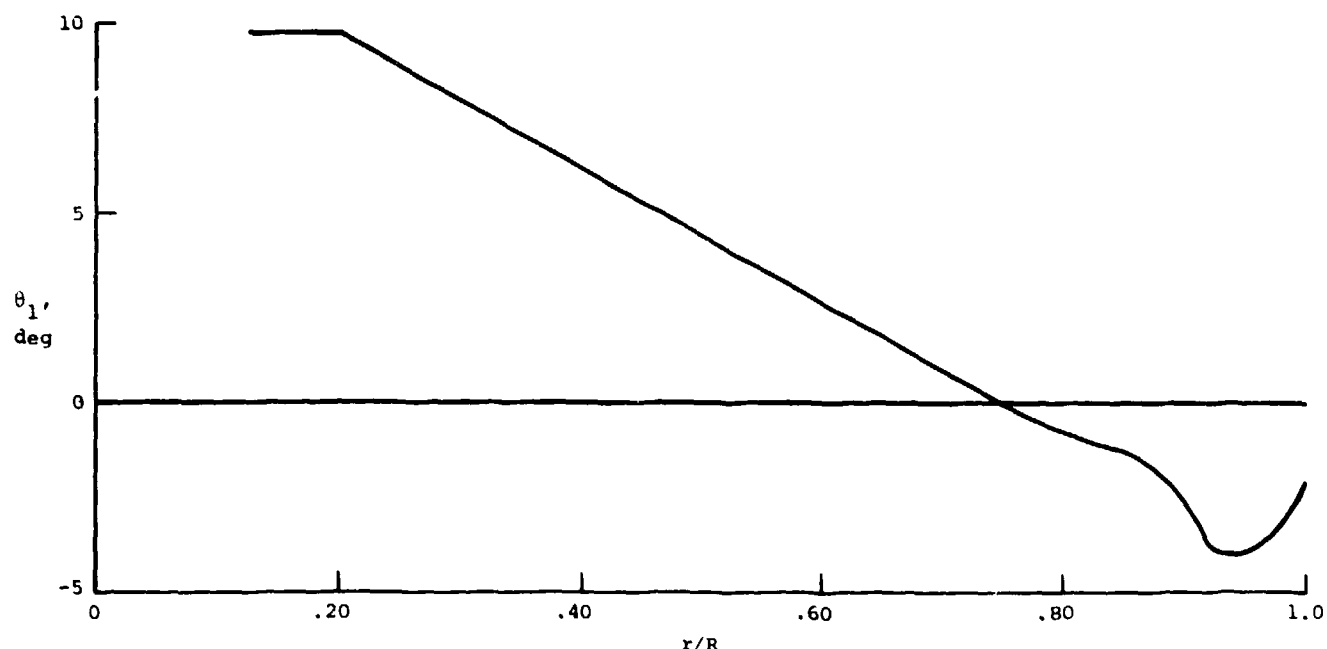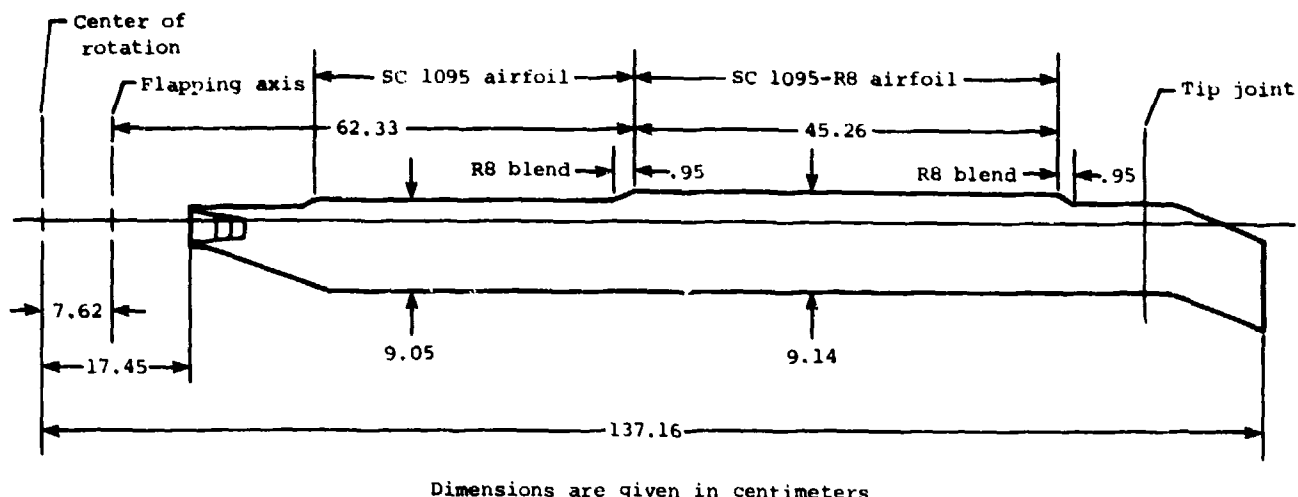
Figure 3.- Rotor blade geometry.

Baseline tip
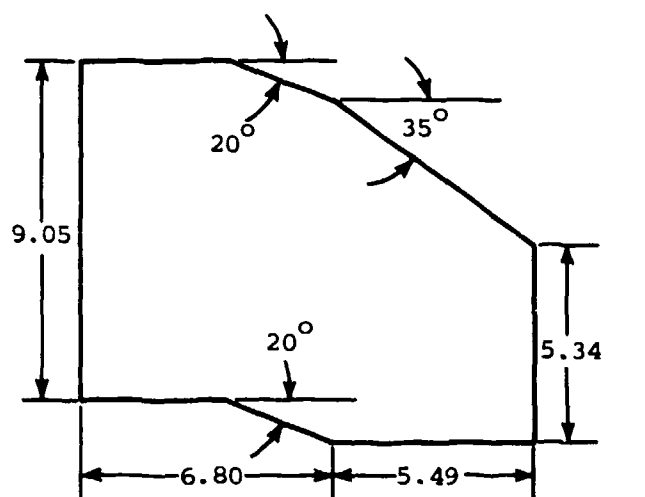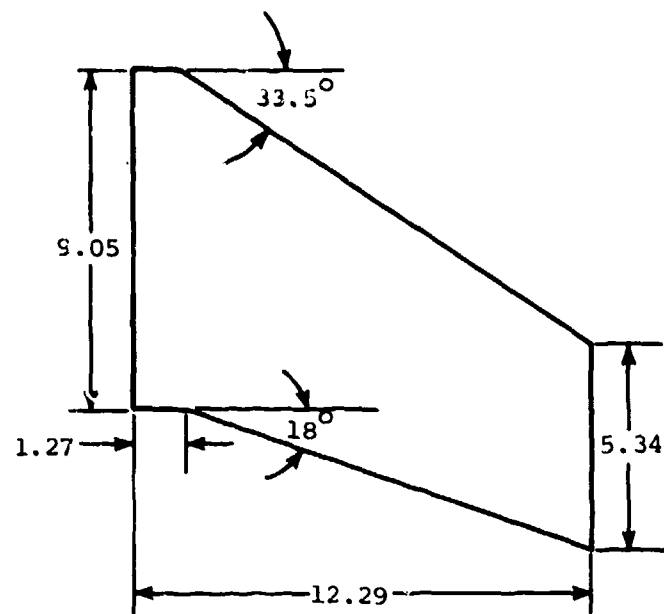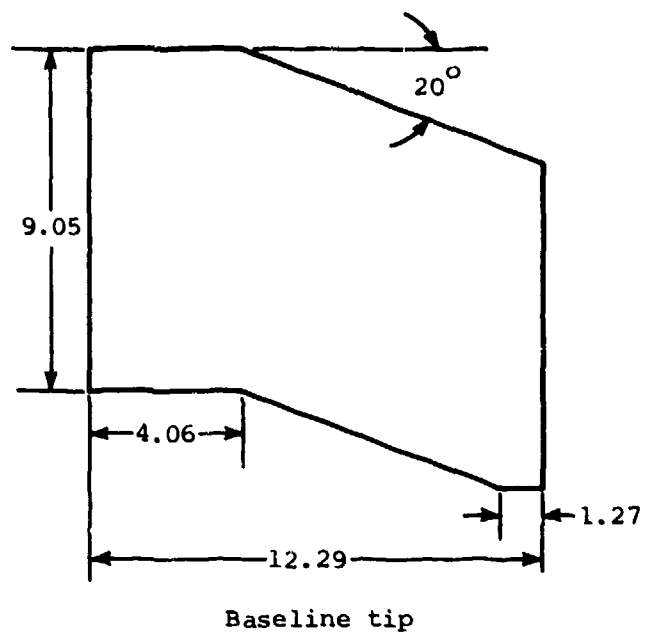
Swept, tapered tip with and without anhedral
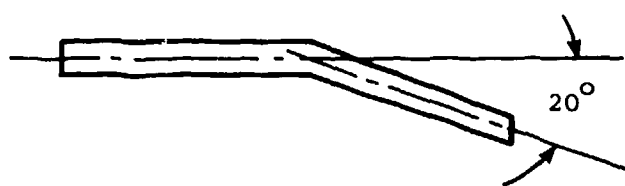
Double-swept tip with anhedral

(a) Tip planforms. Linear dimensions are given in centimeters.

Figure 4.- Tip geometry.
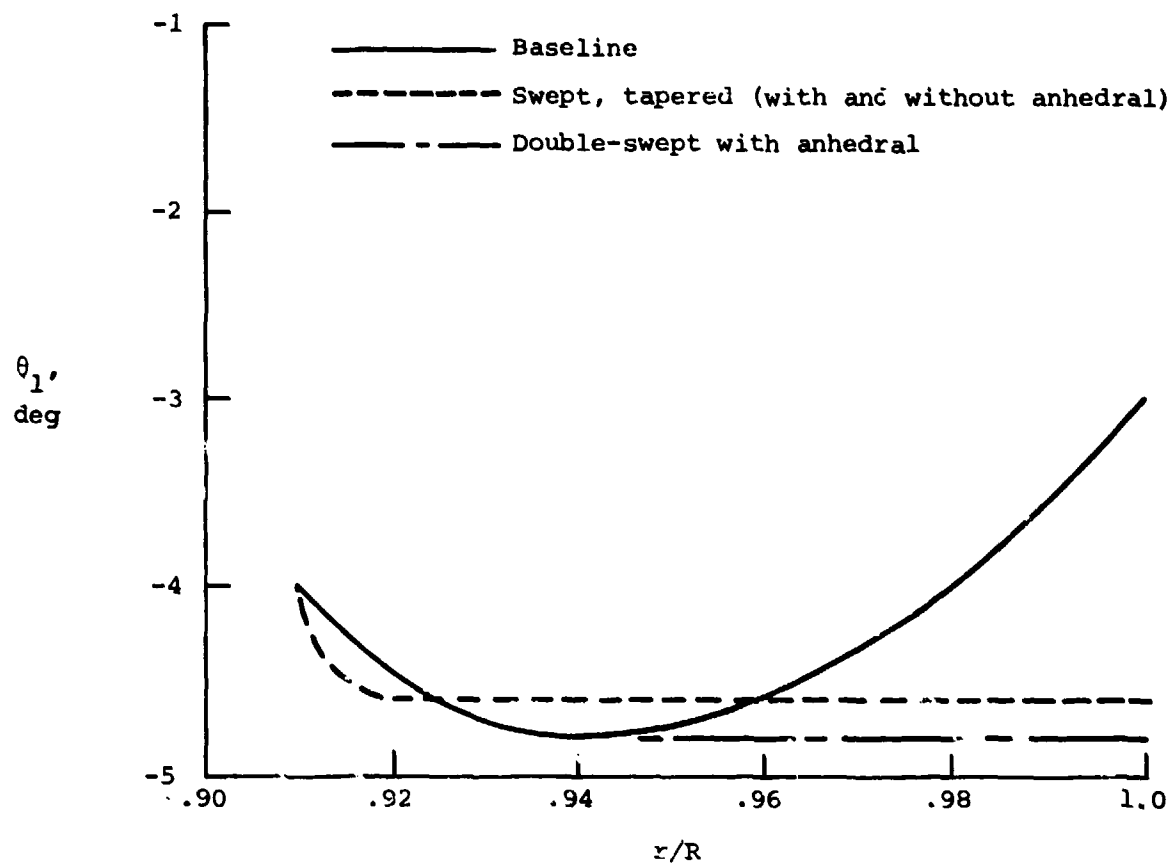
(b) Tip twist distribution (positive nose-up).

Figure 4.- Concluded.

19
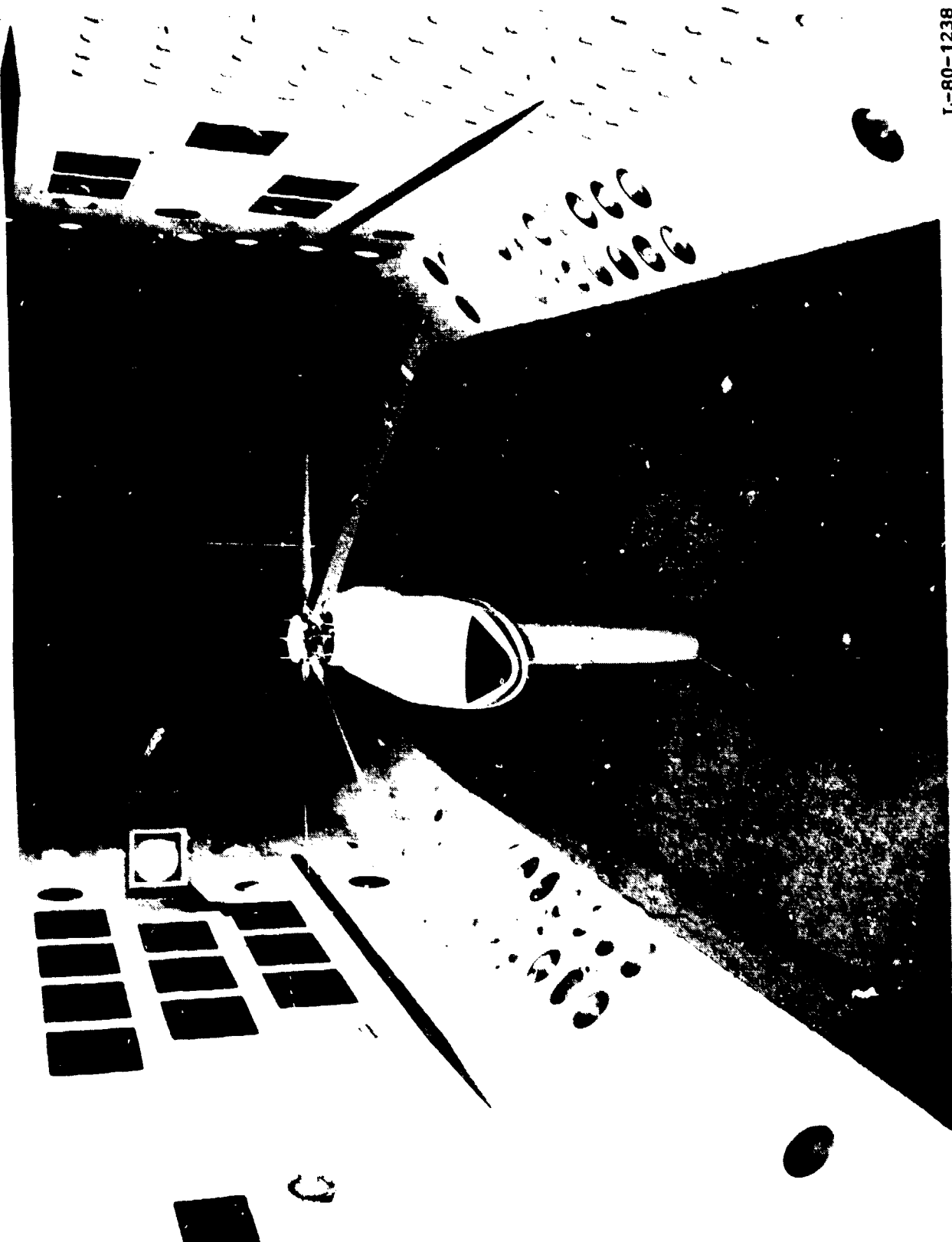
Figure 5.- ARES in TDT.
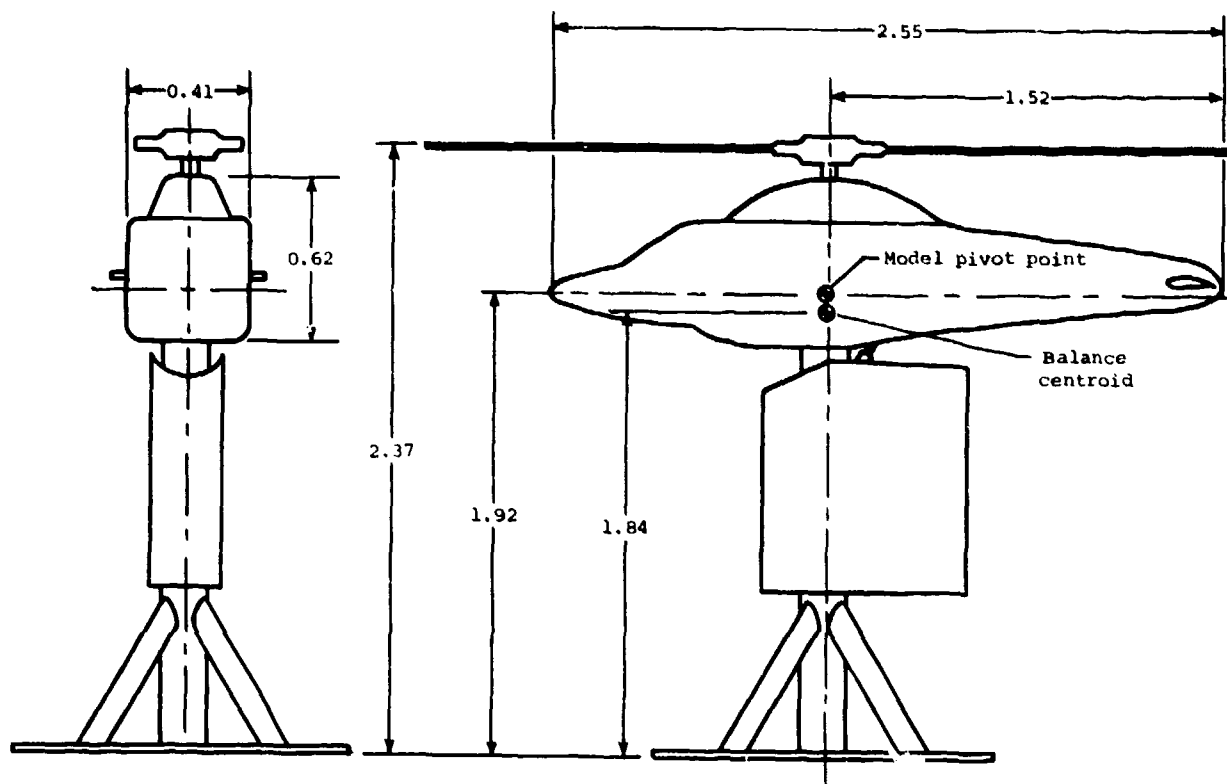
Figure 6.- Schematic diagram of aeroelastic rotor experimental system. All dimensions are given in meters.
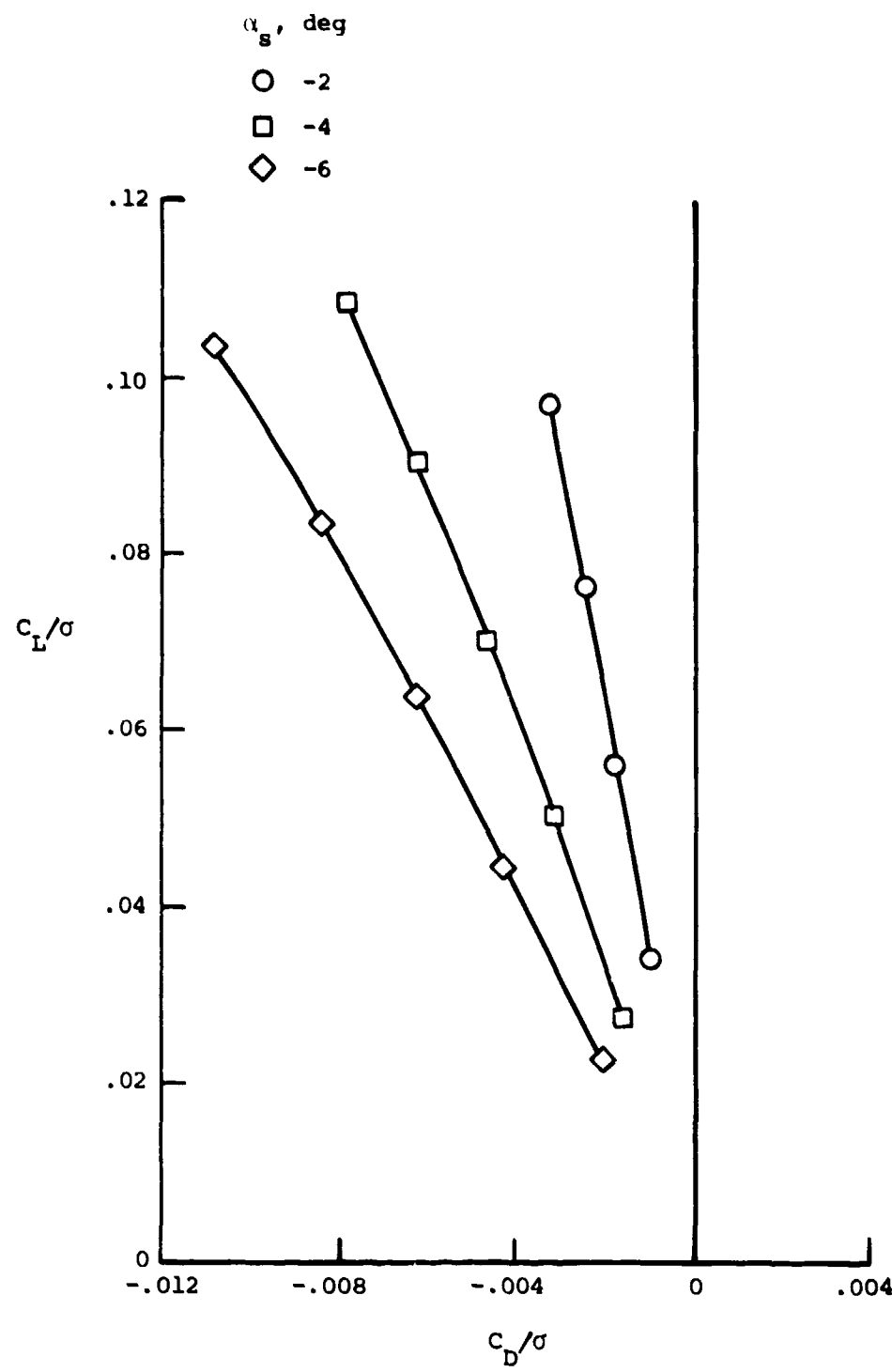
(a) C_L/σ versus C_D/σ at $\mu = 0.20$.

Figure 7.- Basic rotor experimental data for baseline tip.

22
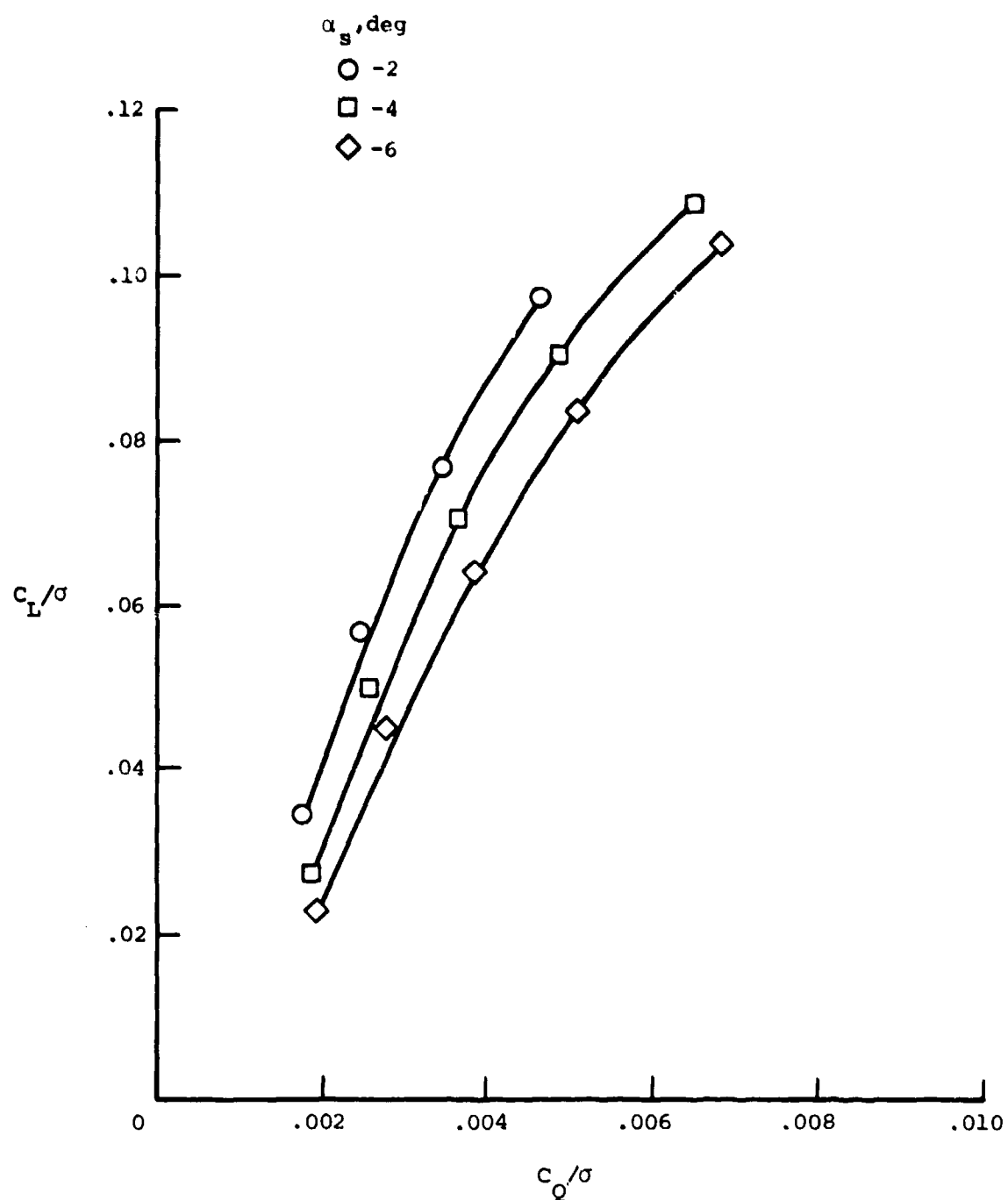
(b) C_L/σ versus C_Q/σ at $\mu = 0.20$.

Figure 7.- Continued.

(c) C_L/σ versus C_D/σ at $\mu = 0.30$.

Figure 7.- Continued.

24

(d) C_L/σ versus C_Q/σ at $\mu = 0.30$.
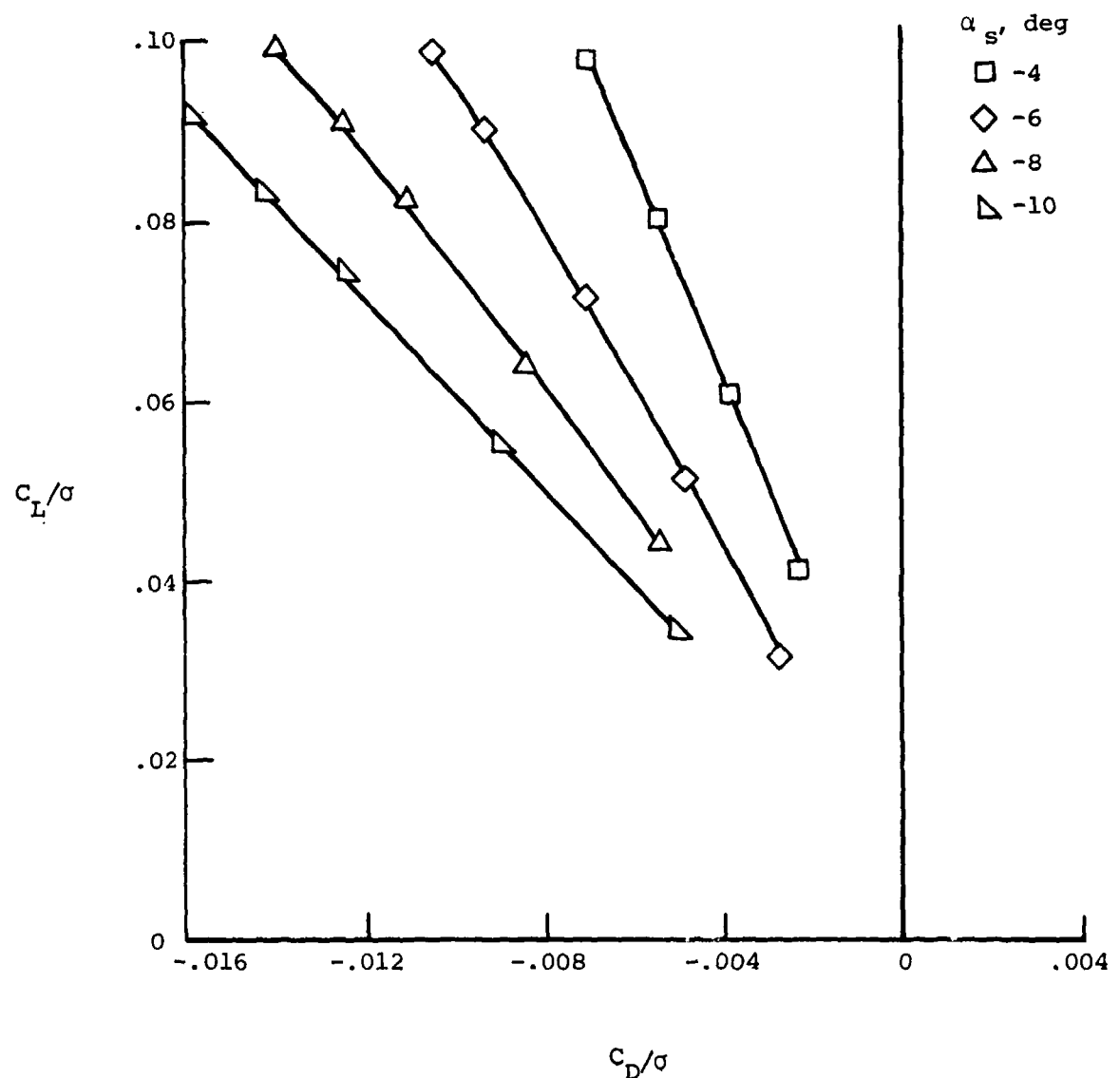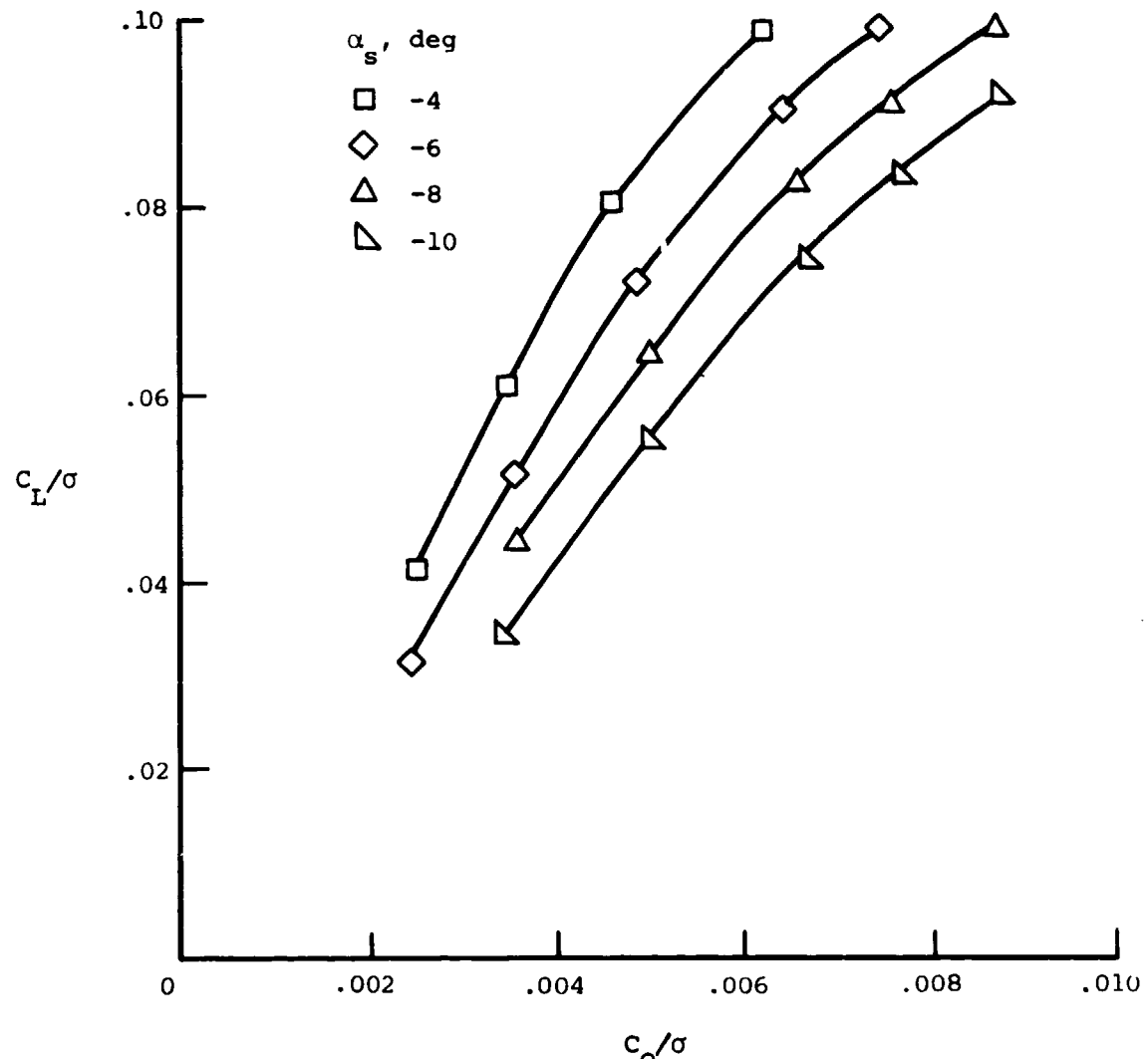
Figure 7.- Continued.
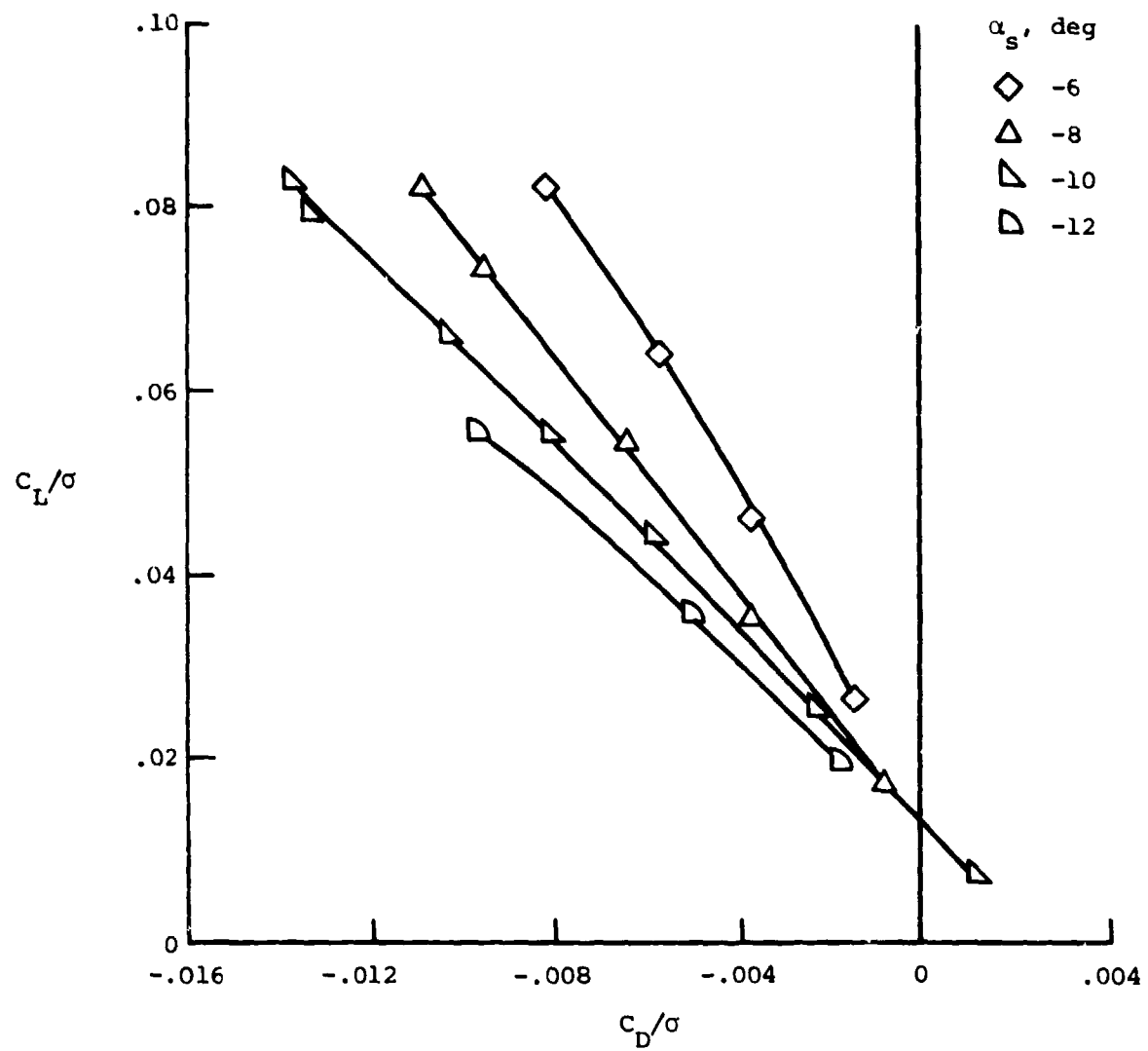
(e) C_L/σ versus C_D/σ at $\mu = 0.35$.

Figure 7.- Continued.
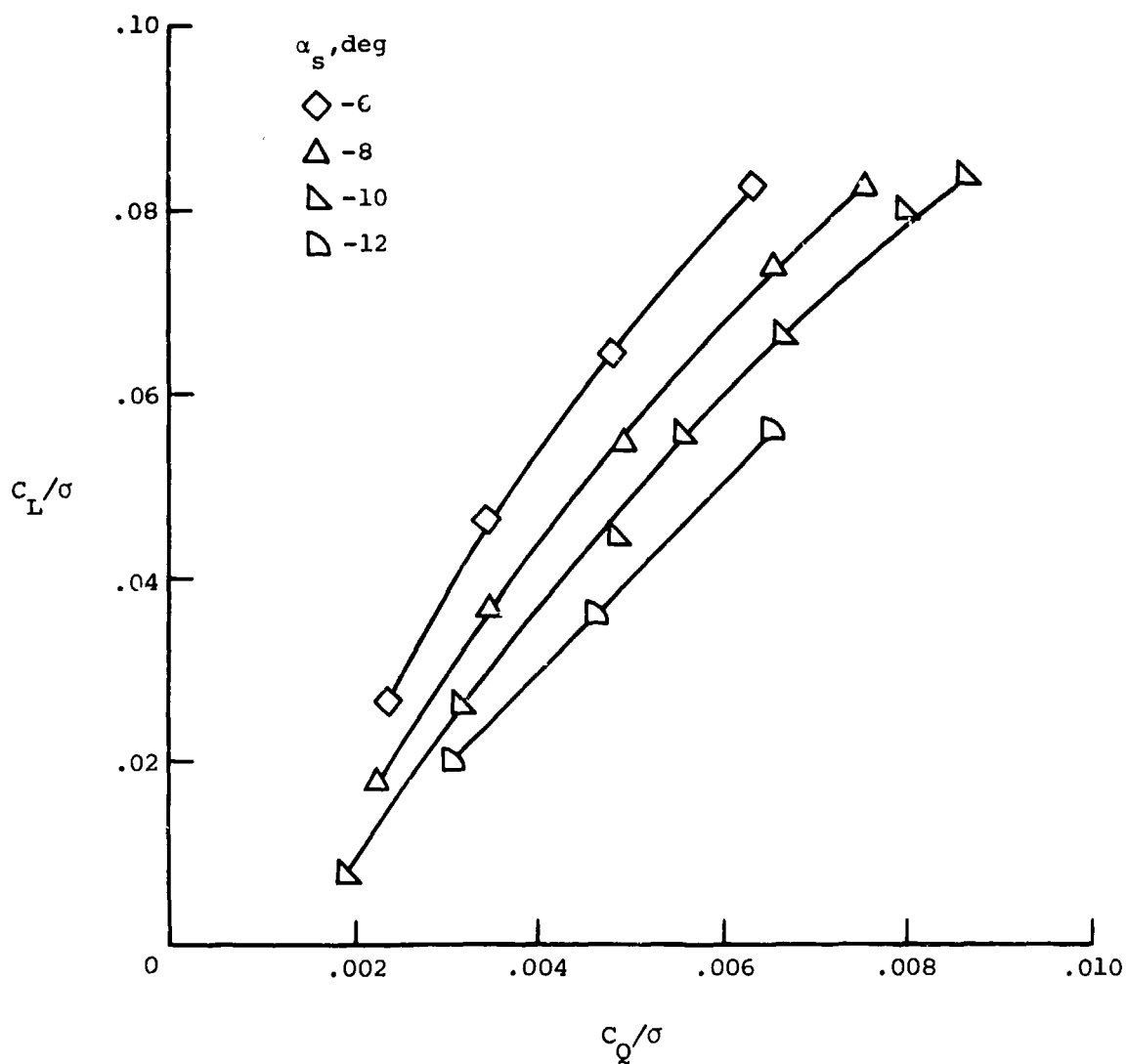
(f) C_L/σ versus C_Q/σ at $\mu = 0.35$.

Figure 7.- Concluded.
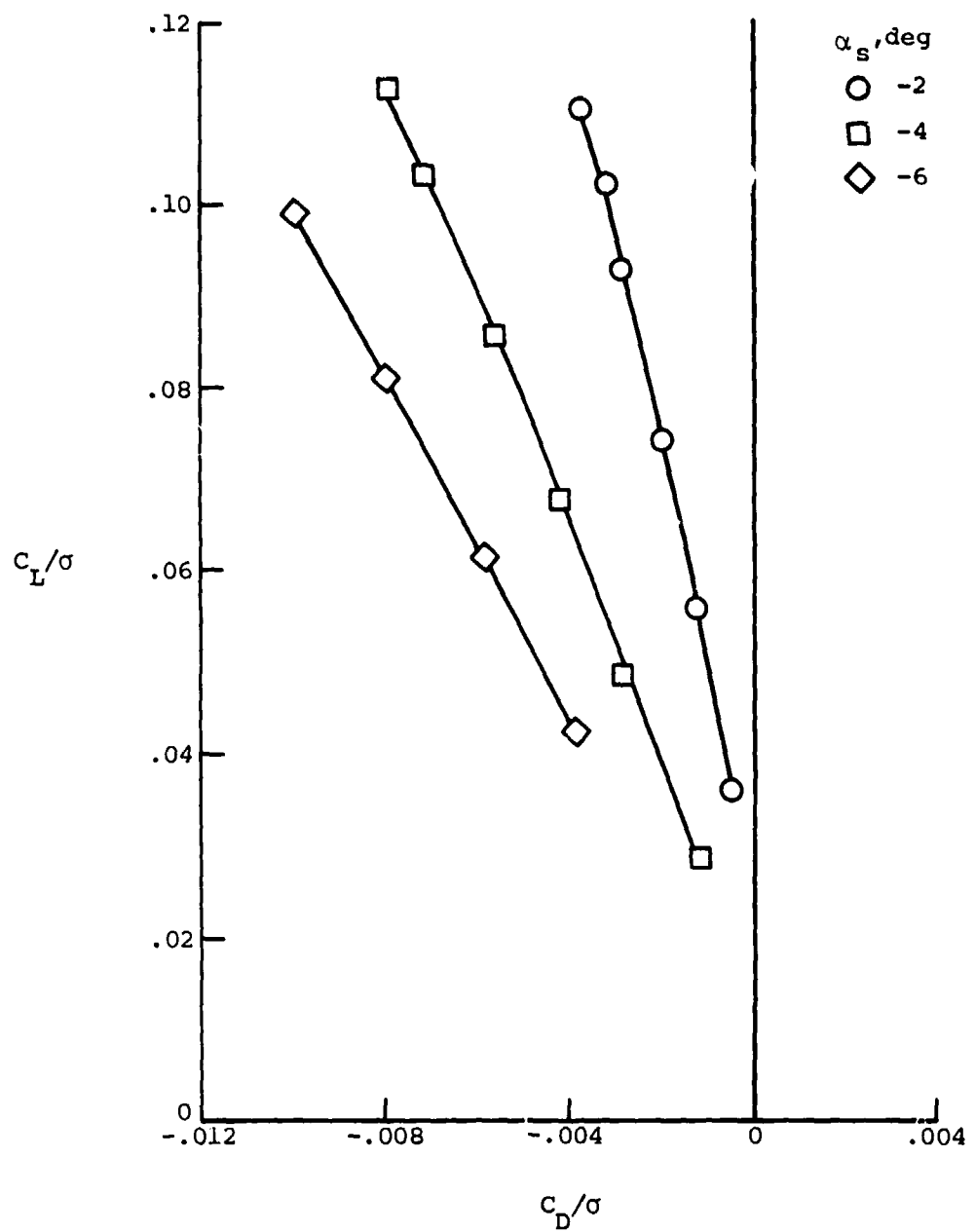
(a) C_L/σ versus C_D/σ at $\mu = 0.20$.

Figure 8.- Basic rotor experimental data swept, tapered tip.
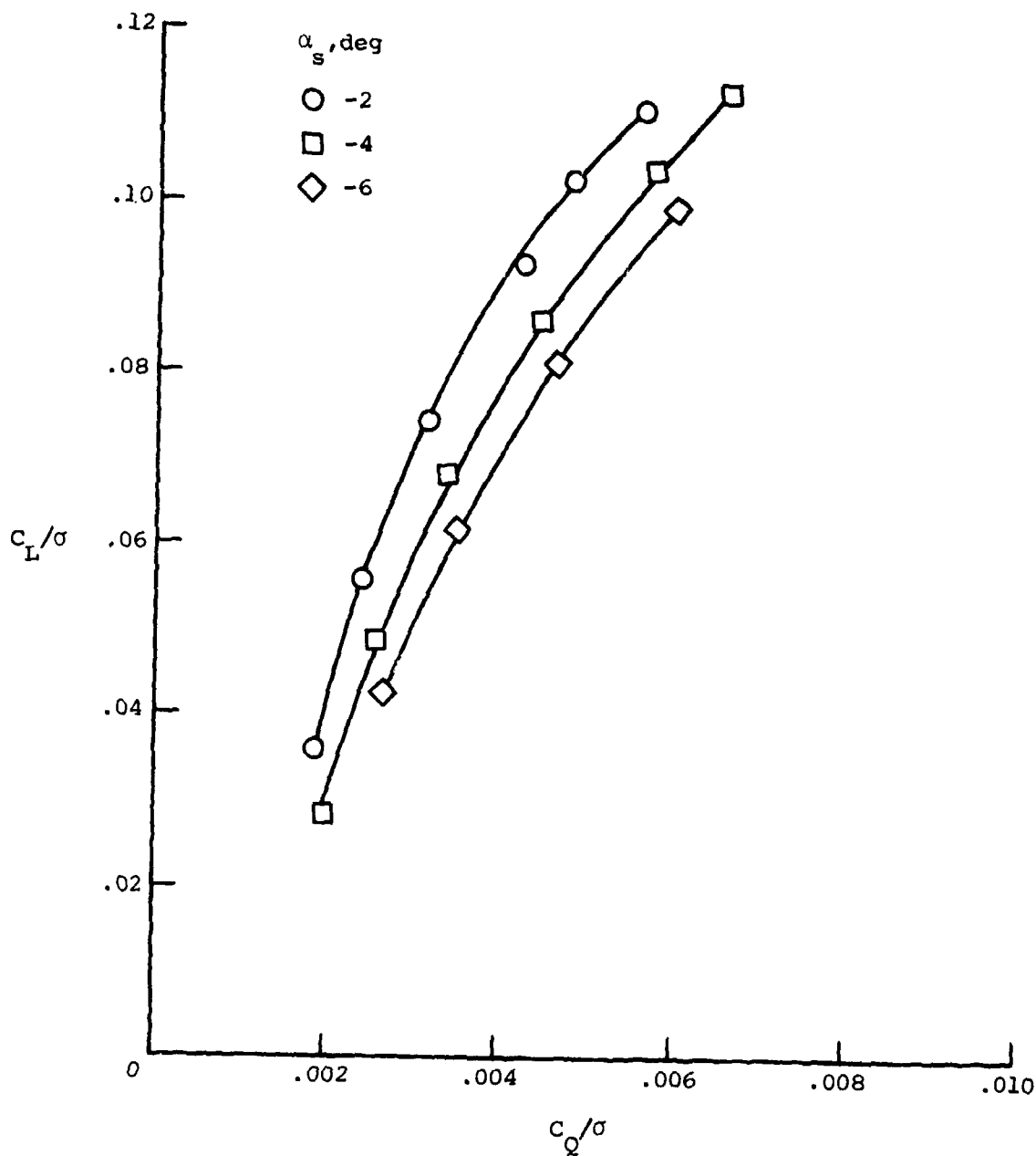
(b) C_L/σ versus C_Q/σ at $\mu = 0.20$.

Figure 8.- Continued.
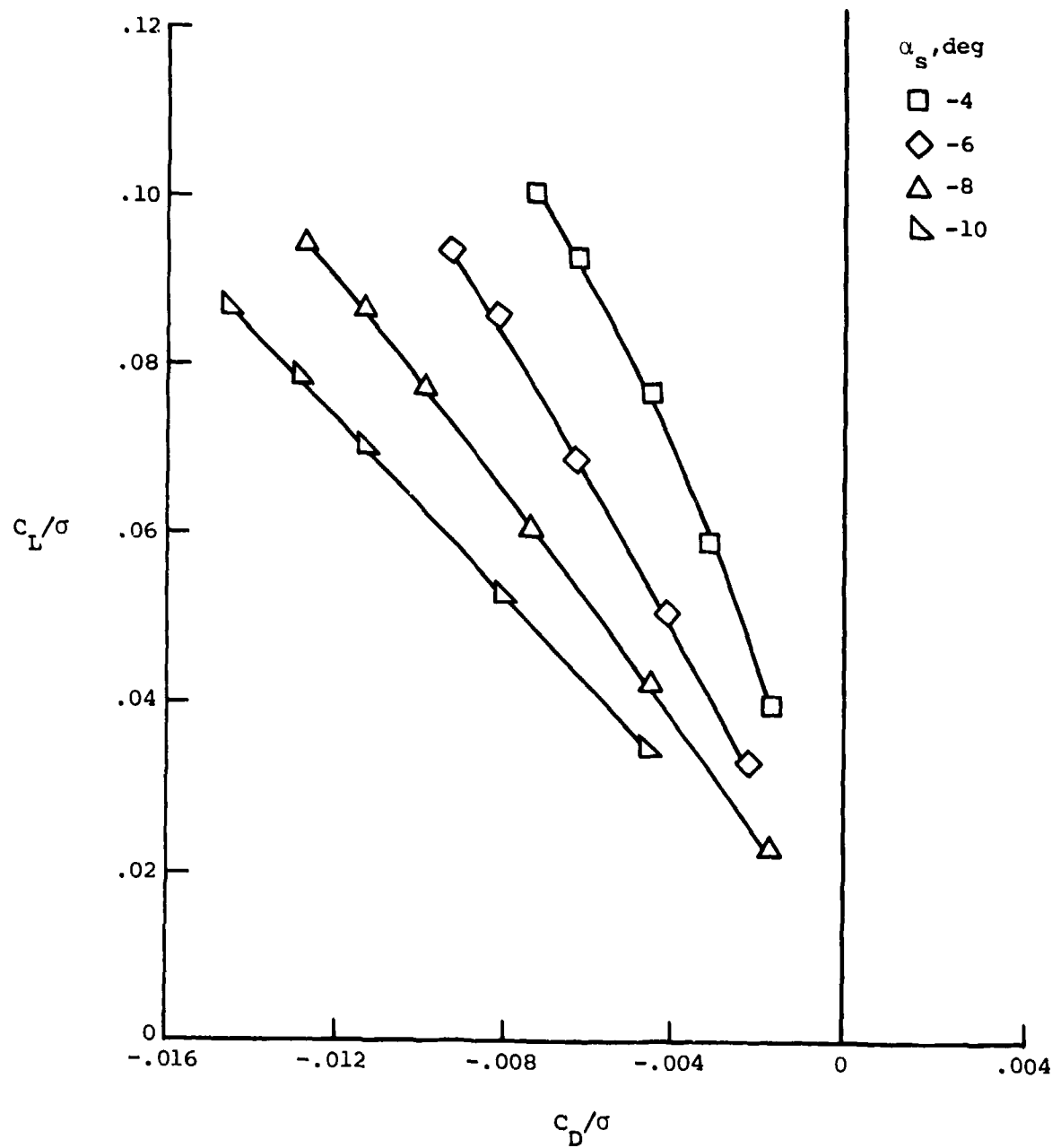
29

(c) C_L/σ versus C_D/σ at $\mu = 0.30$.

Figure 8.- Continued.

30

(d) C_L/σ versus C_Q/σ at $\mu = 0.30$.

Figure 8.- Continued.

31
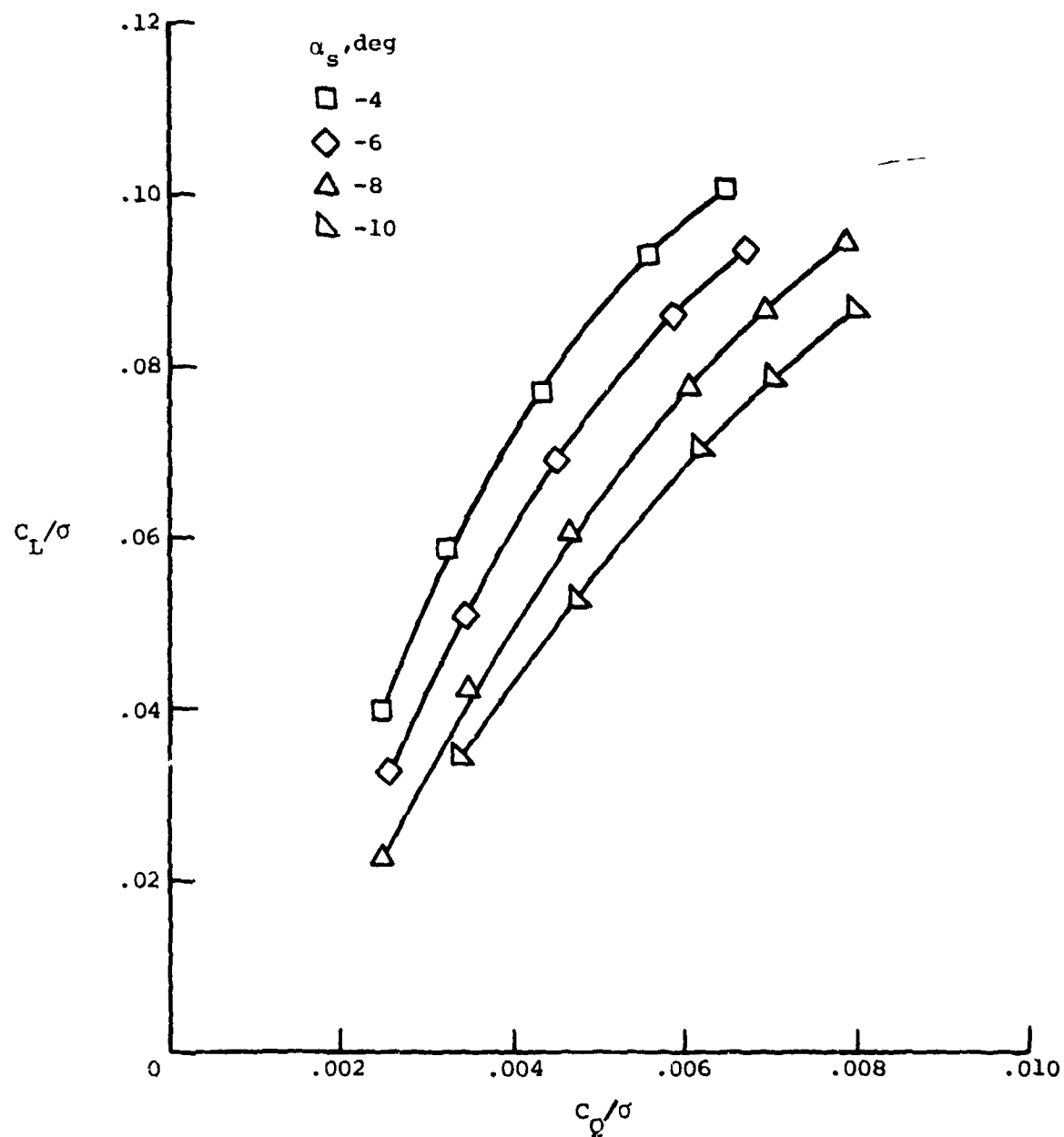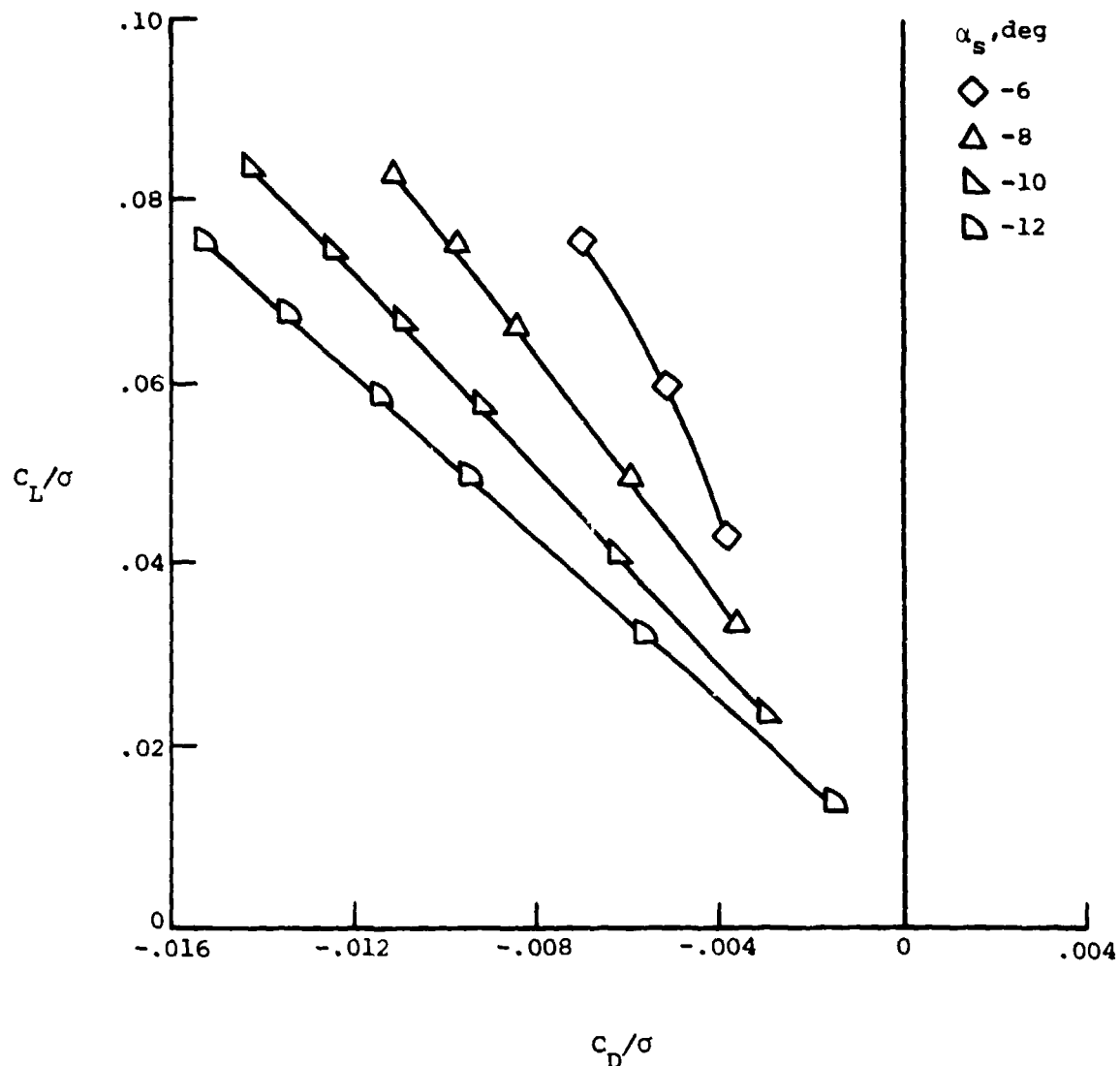
(e) C_L/σ versus C_D/σ at $\mu = 0.35$.

Figure 8.- Continued.

32
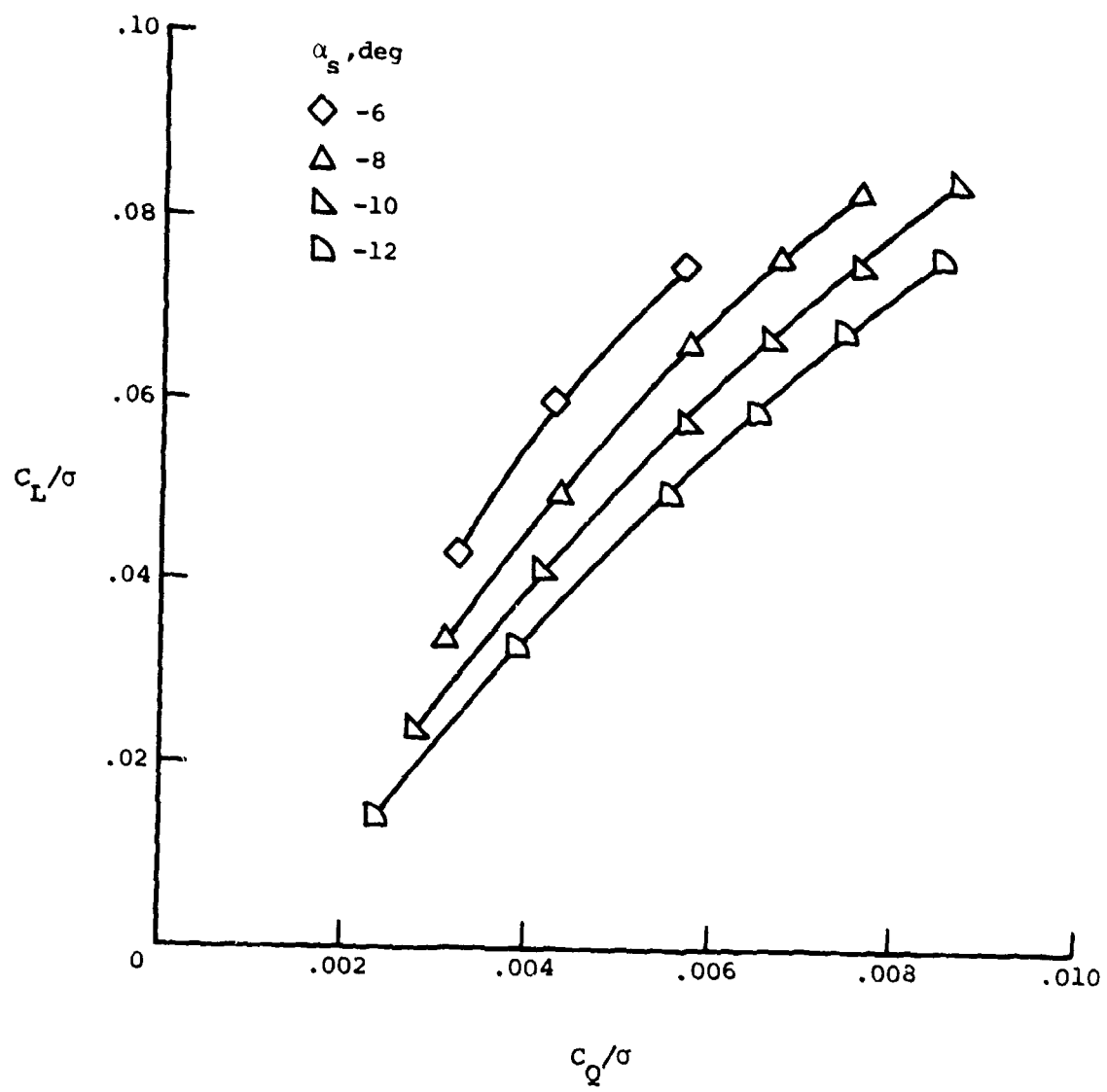
(f) C_L/σ versus C_Q/σ at $\mu = 0.35$.

Figure 8.- Concluded.

33
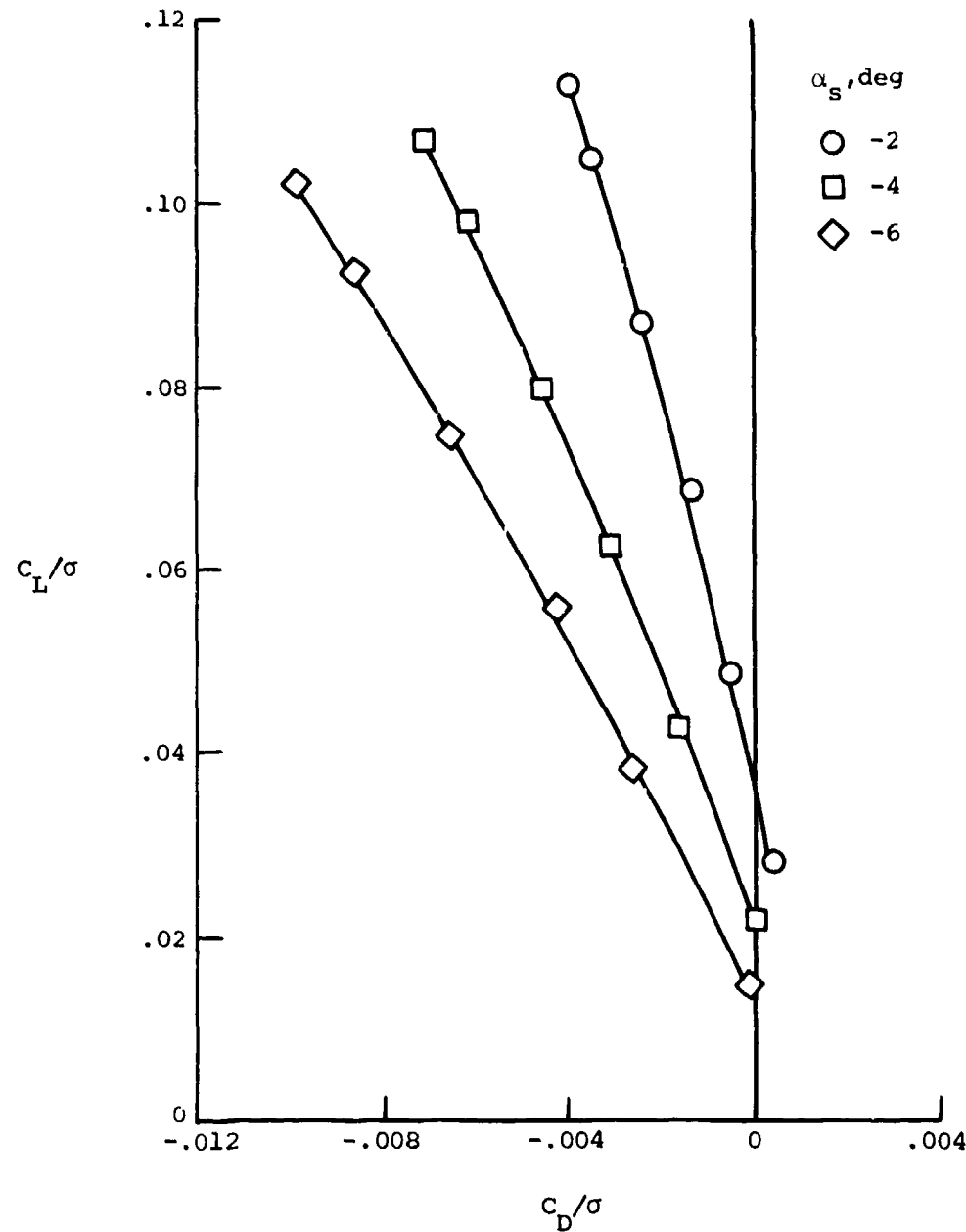
(a) C_L/σ versus C_D/σ at $\mu = 0.20$.

Figure 9.- Basic rotor experimental data for swept, tapered tip with anhedral.
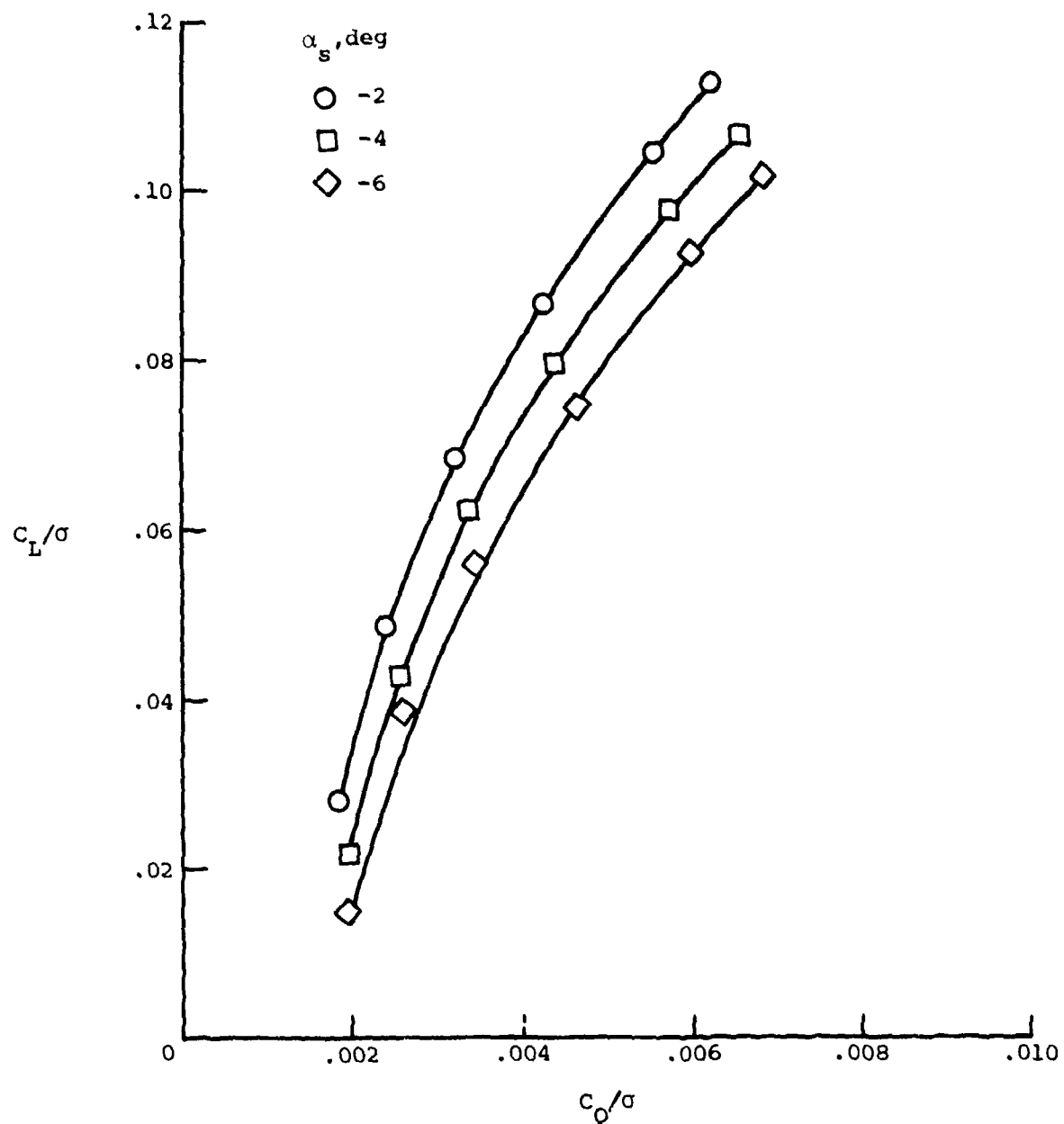
(b) C_L/σ versus C_Q/σ at $\mu = 0.20$.

Figure 9.- Continued.

(c) C_L/σ versus C_D/σ at $\mu = 0.30$.

Figure 9.- Continued.

36

(d) C_L/σ versus C_Q/σ at $\mu = 0.30$.
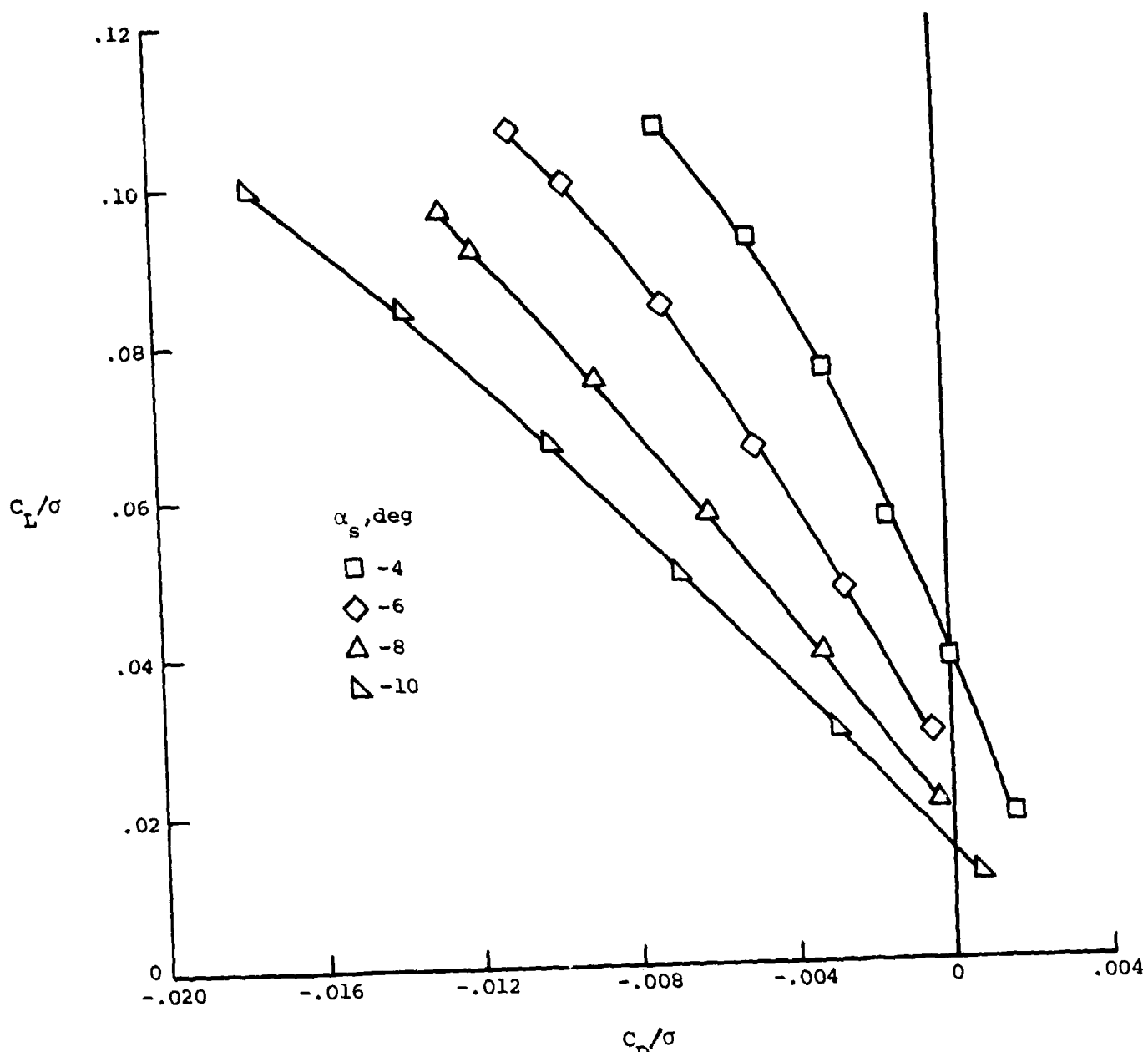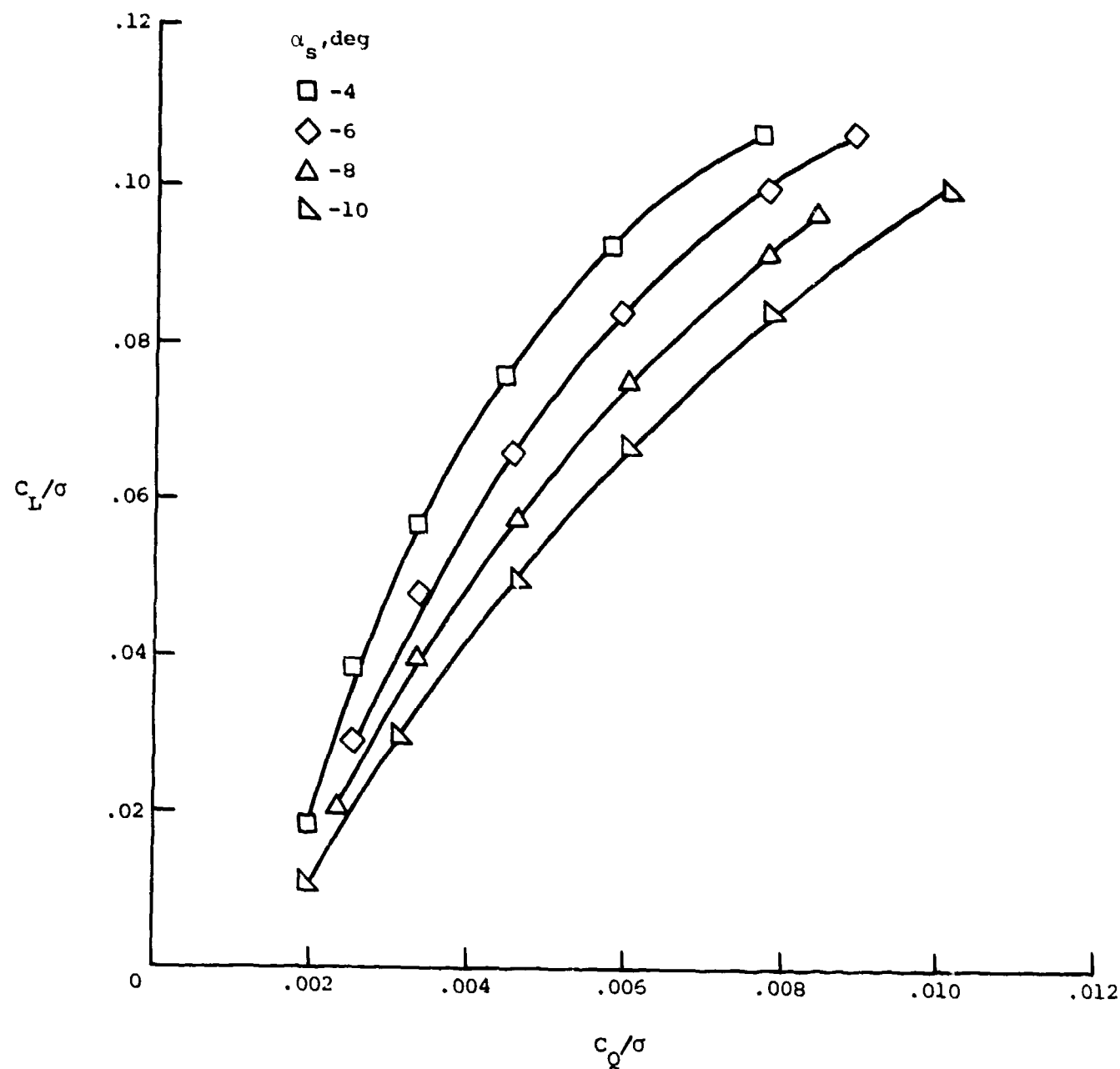
Figure 9.- Continued.
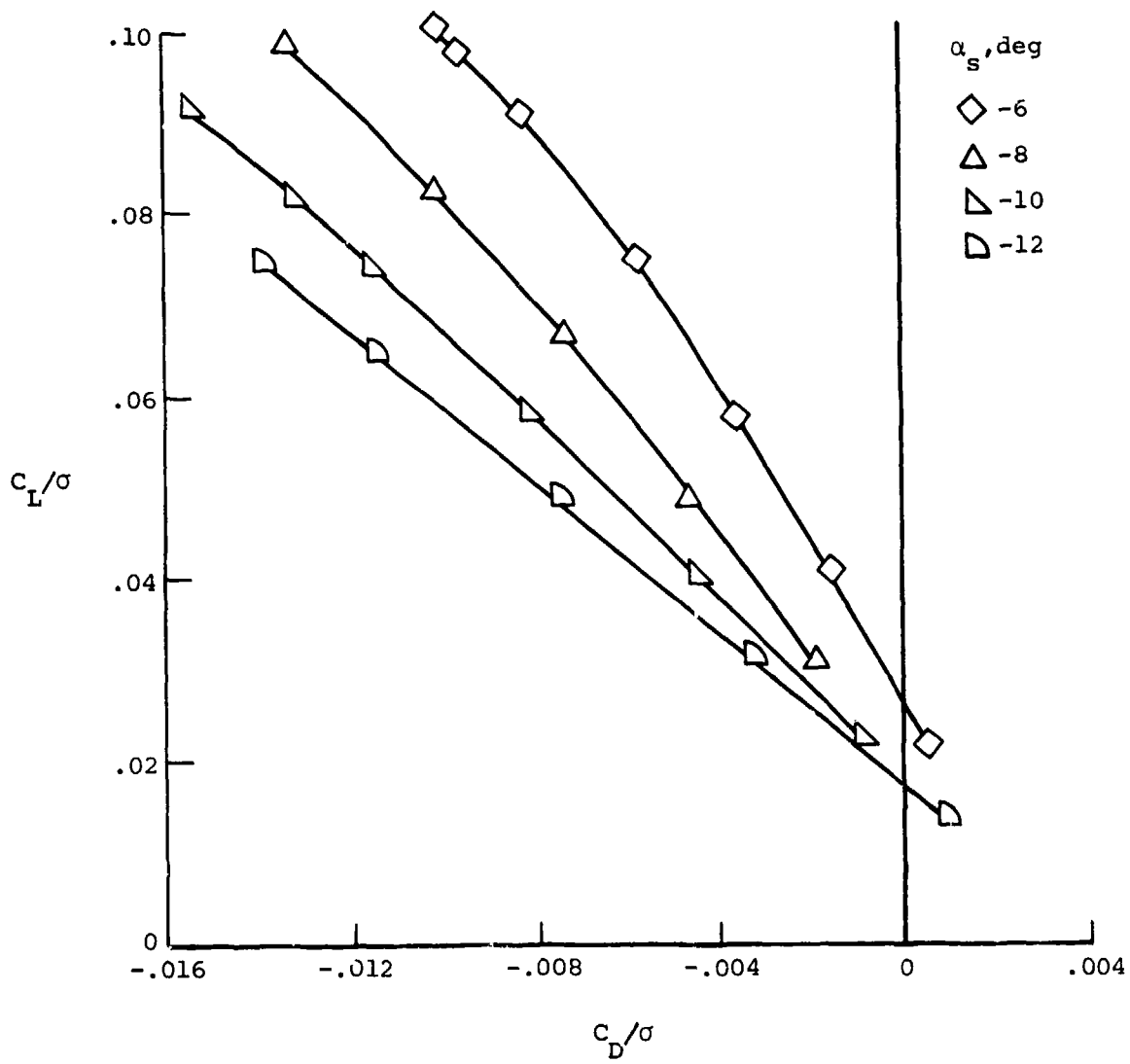
(e) C_L/σ versus C_D/σ at $\mu = 0.35$.

Figure 9.- Continued.

38
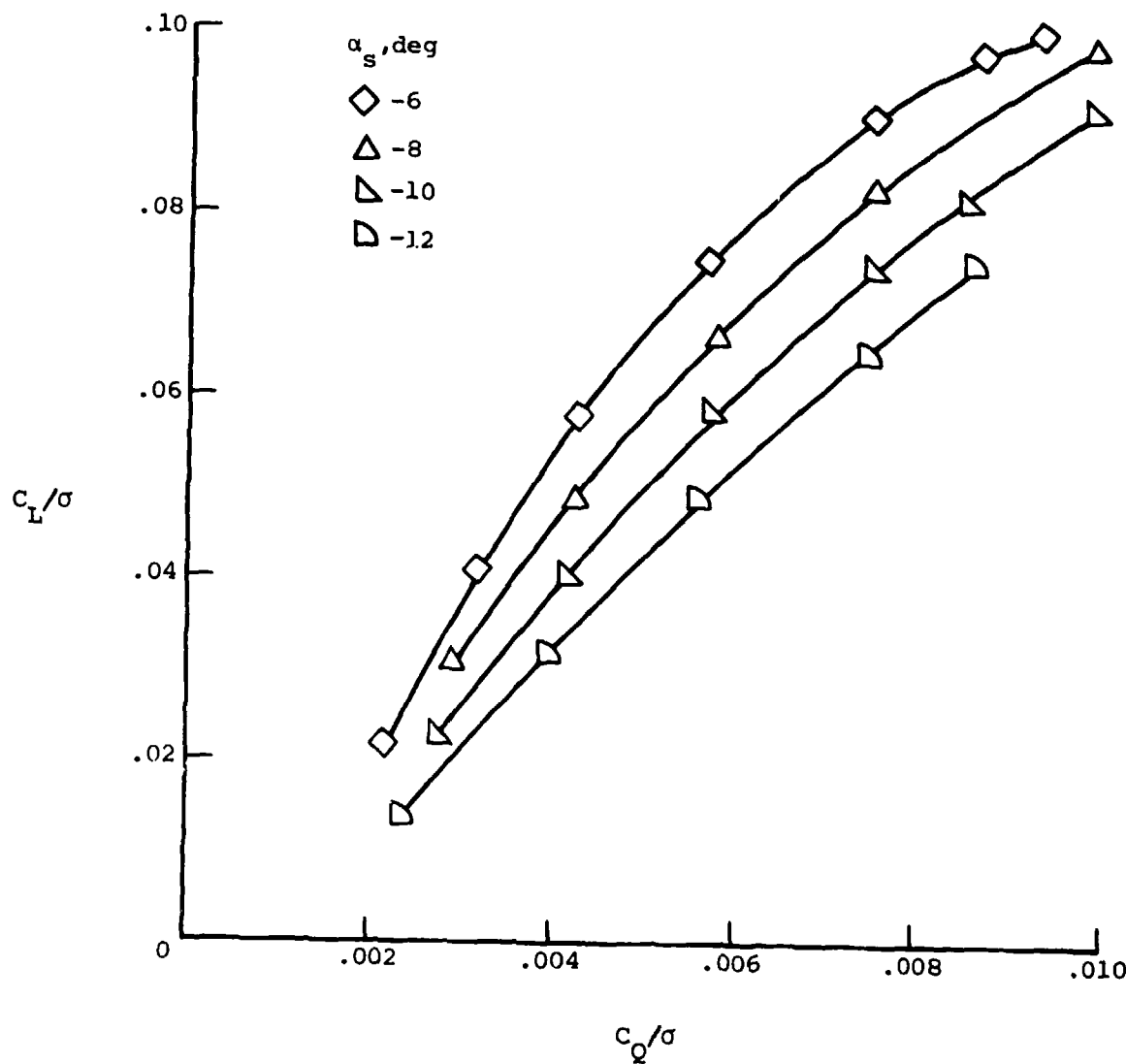
(f) C_L/σ versus C_Q/σ at $\mu = 0.35$.

Figure 9.- Concluded.
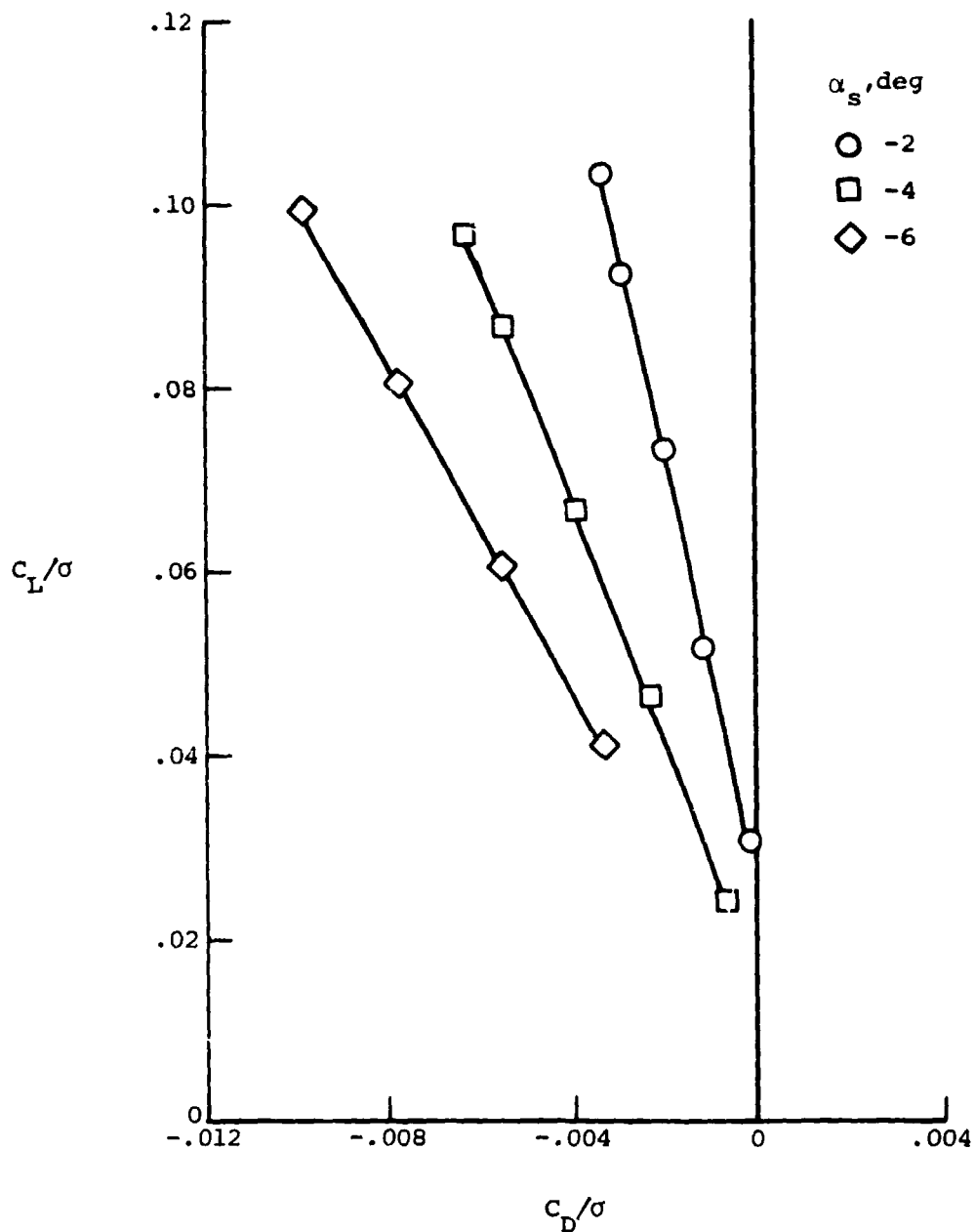
(a) C_L/σ versus C_D/σ at $\mu = 0.20$.

Figure 10.- Basic rotor experimental data for double-swept tip with anhedral.
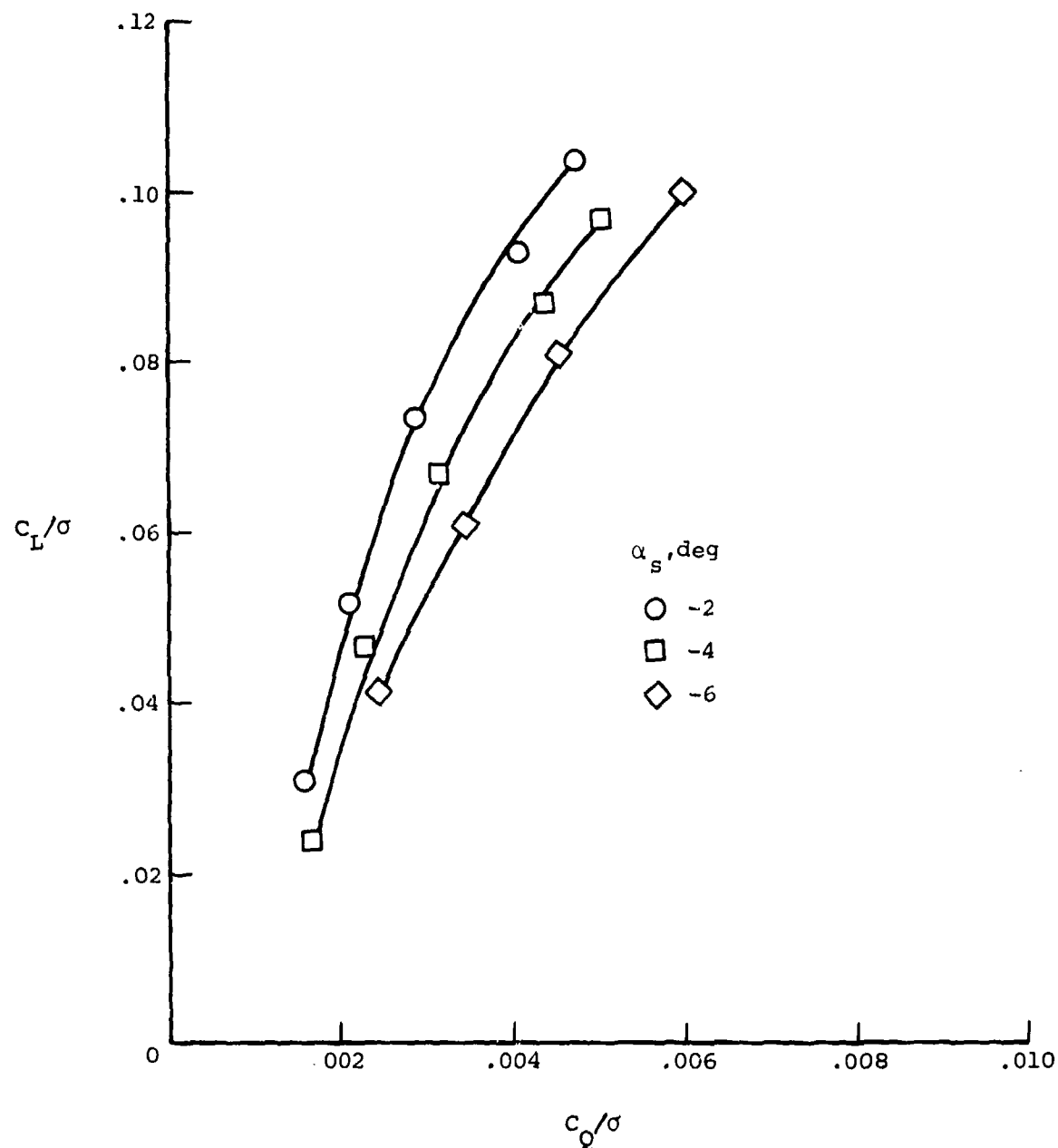
(b) C_L/σ versus C_Q/σ at $\mu = 0.20$.

Figure 10.- Continued.

(c) C_L/σ versus C_D/σ at $\mu = 0.30$.
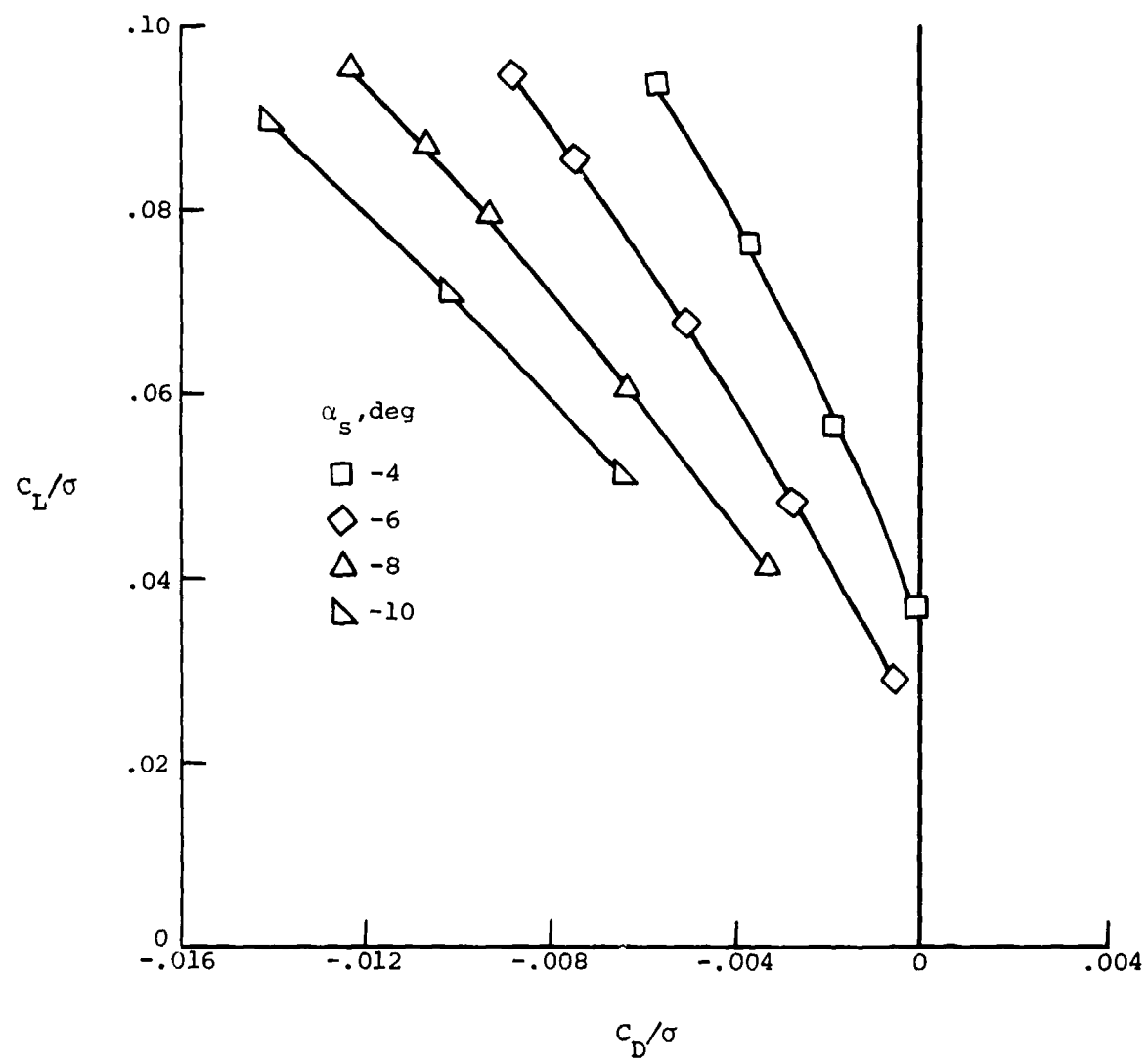
Figure 10.- Continued.

(d) C_L/σ versus C_Q/σ at $\mu = 0.30$.
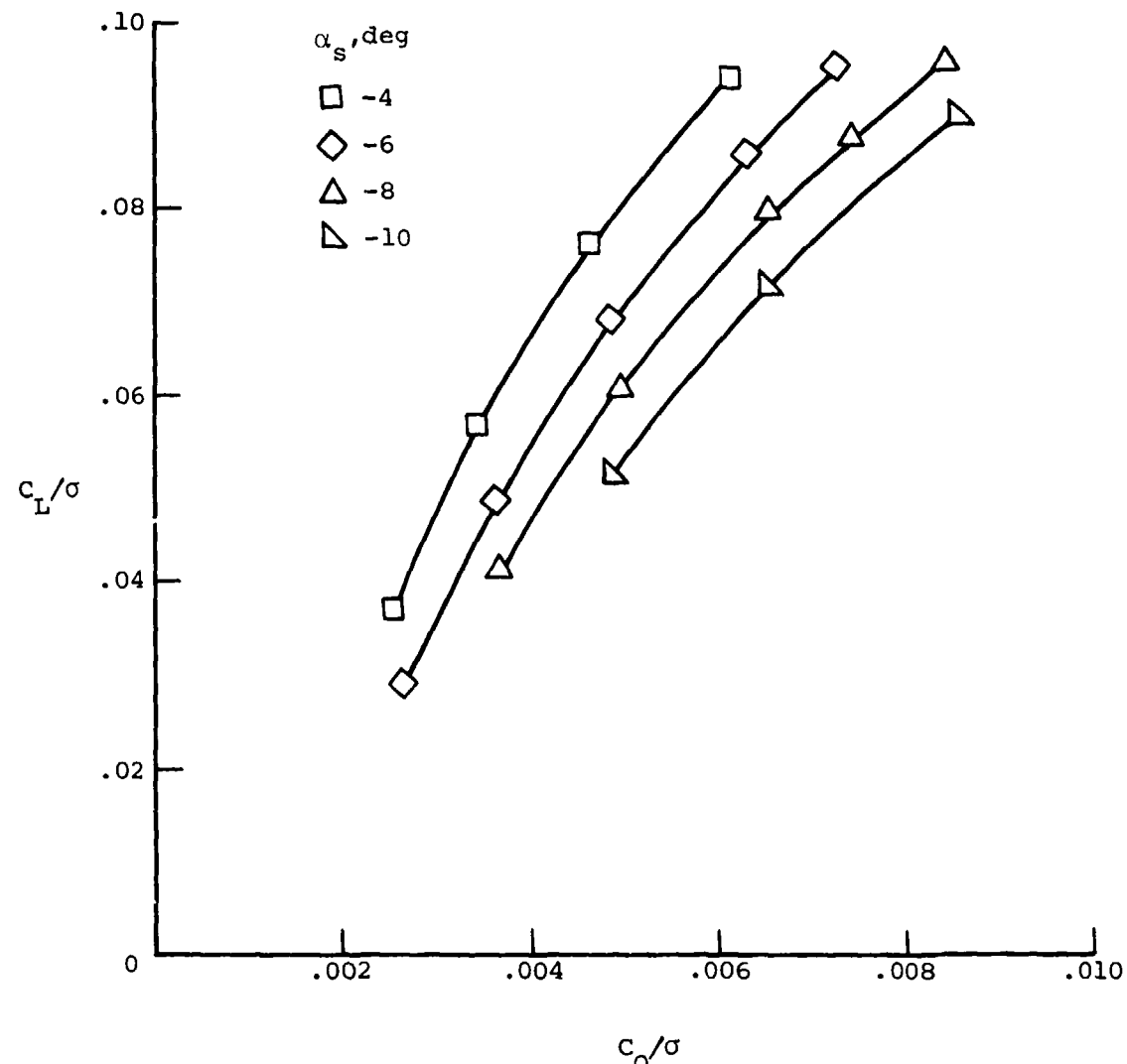
Figure 10.- Continued.
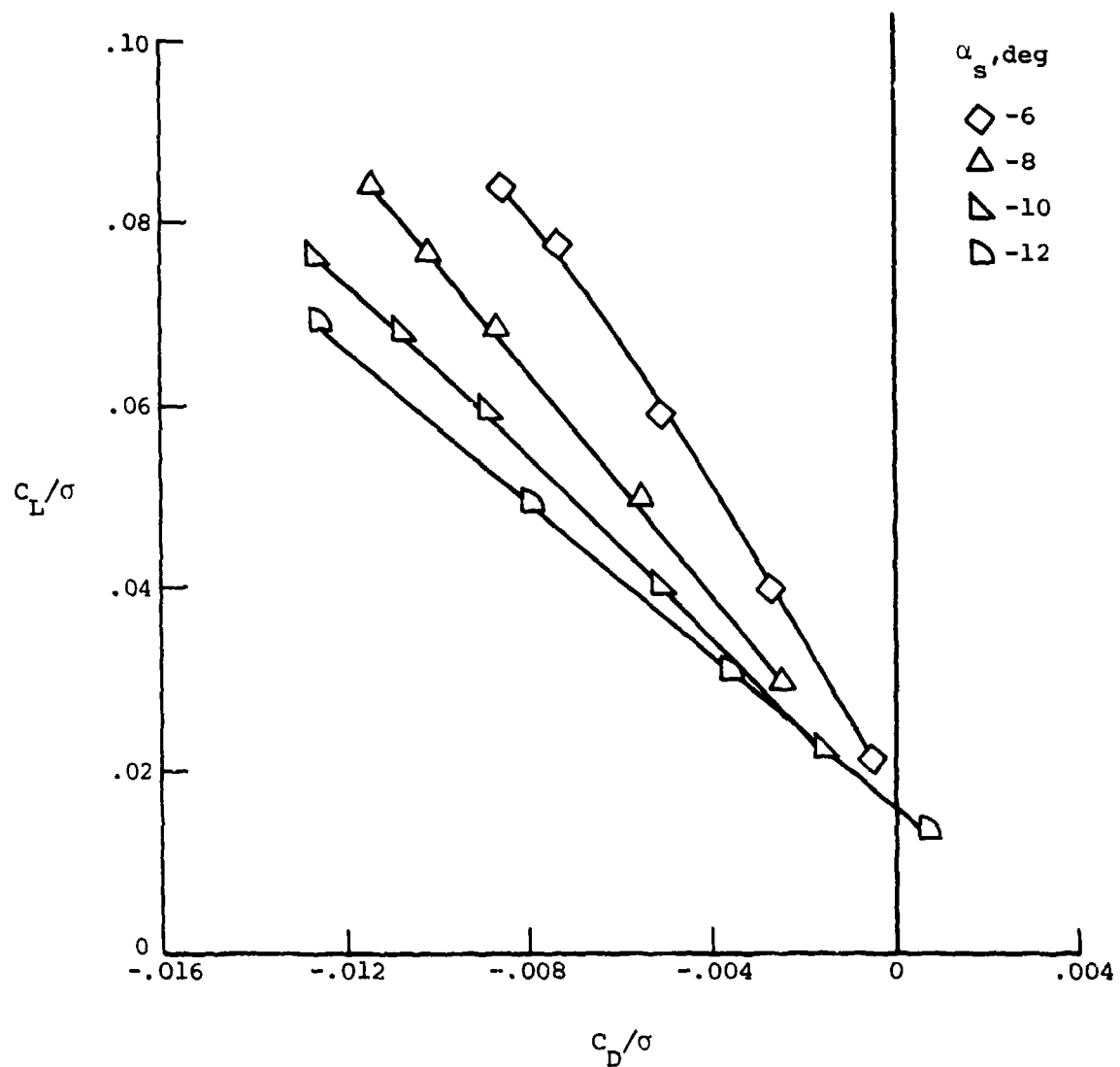
(e) C_L/σ versus C_D/σ at $\mu = 0.35$.

Figure 10.- Continued.

44
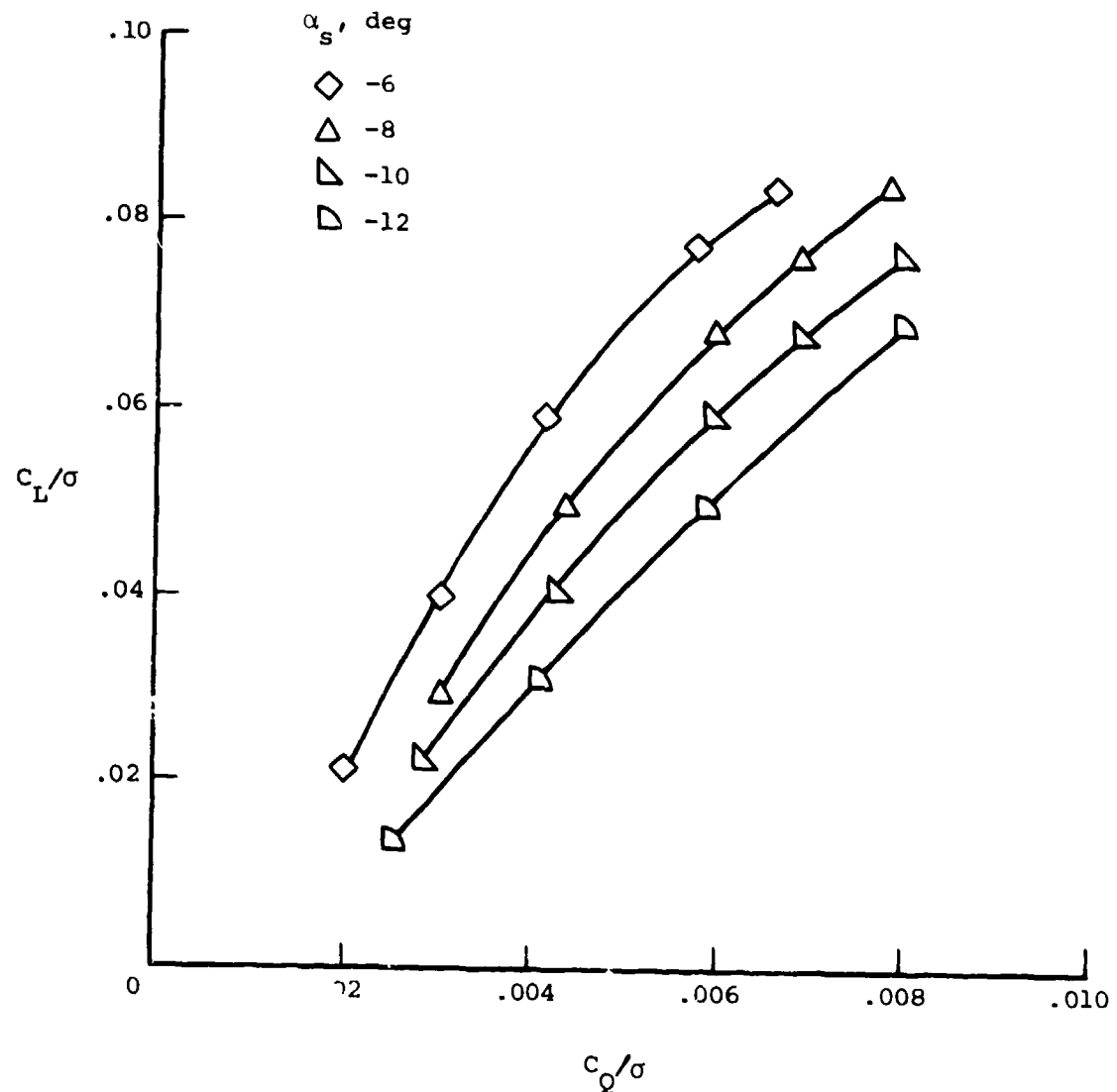
(f) C_L/σ versus C_Q/σ at $\mu = 0.35$.

Figure 10.- Concluded.
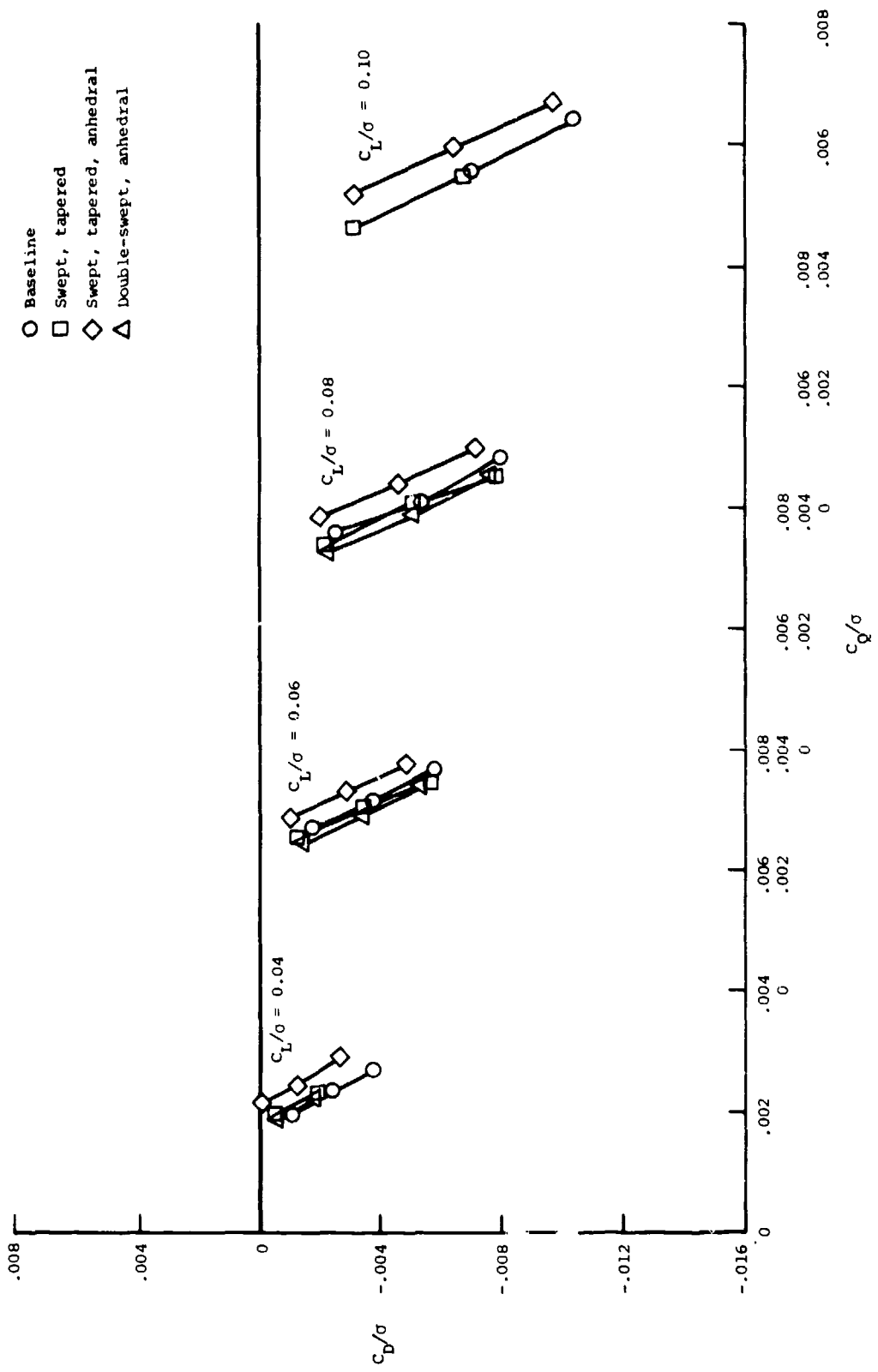
(a) $\mu = 0.20$.

Figure 11.- Experimental rotor performance.
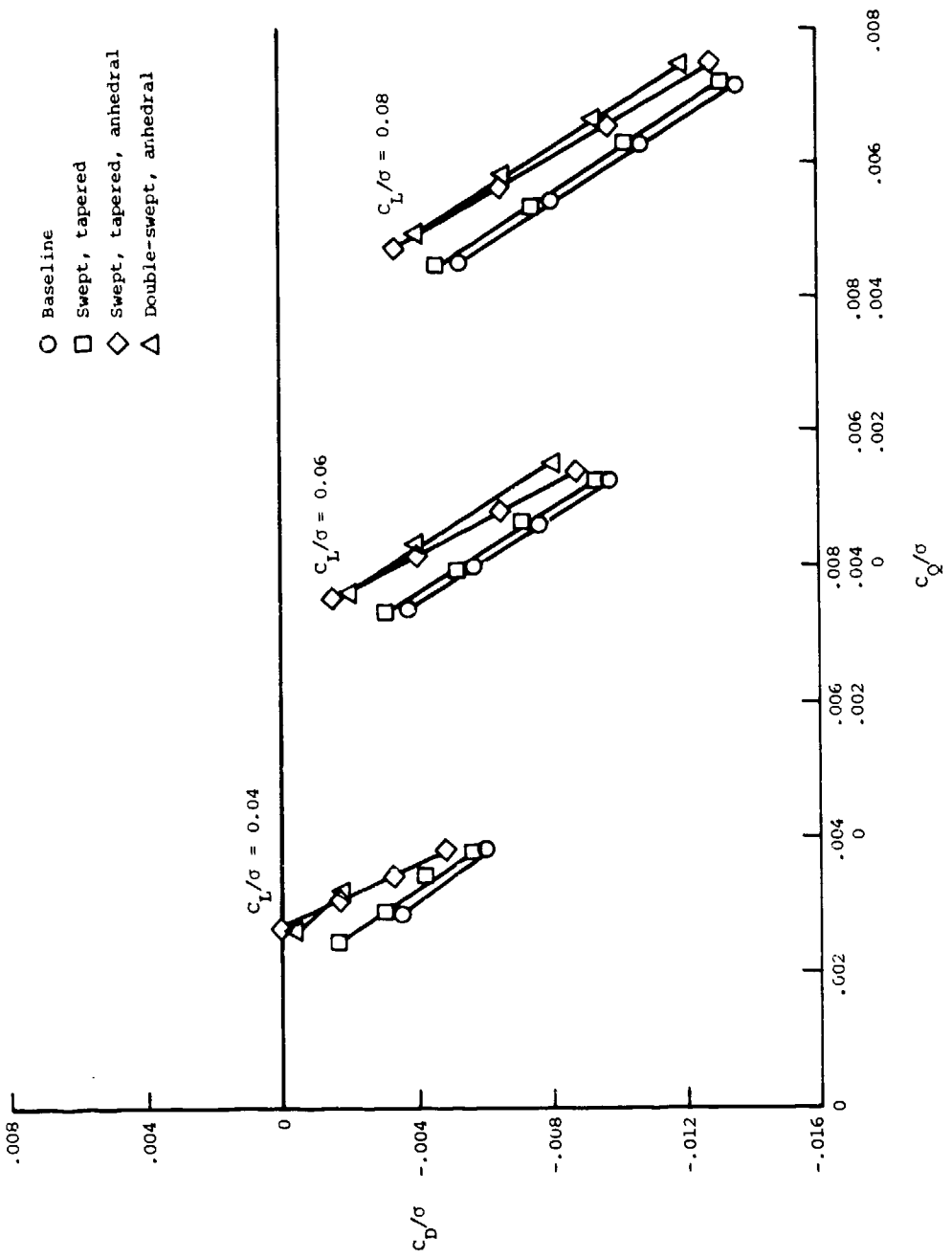
(b) $\mu = 0.30$.

Figure 11.- Continued.
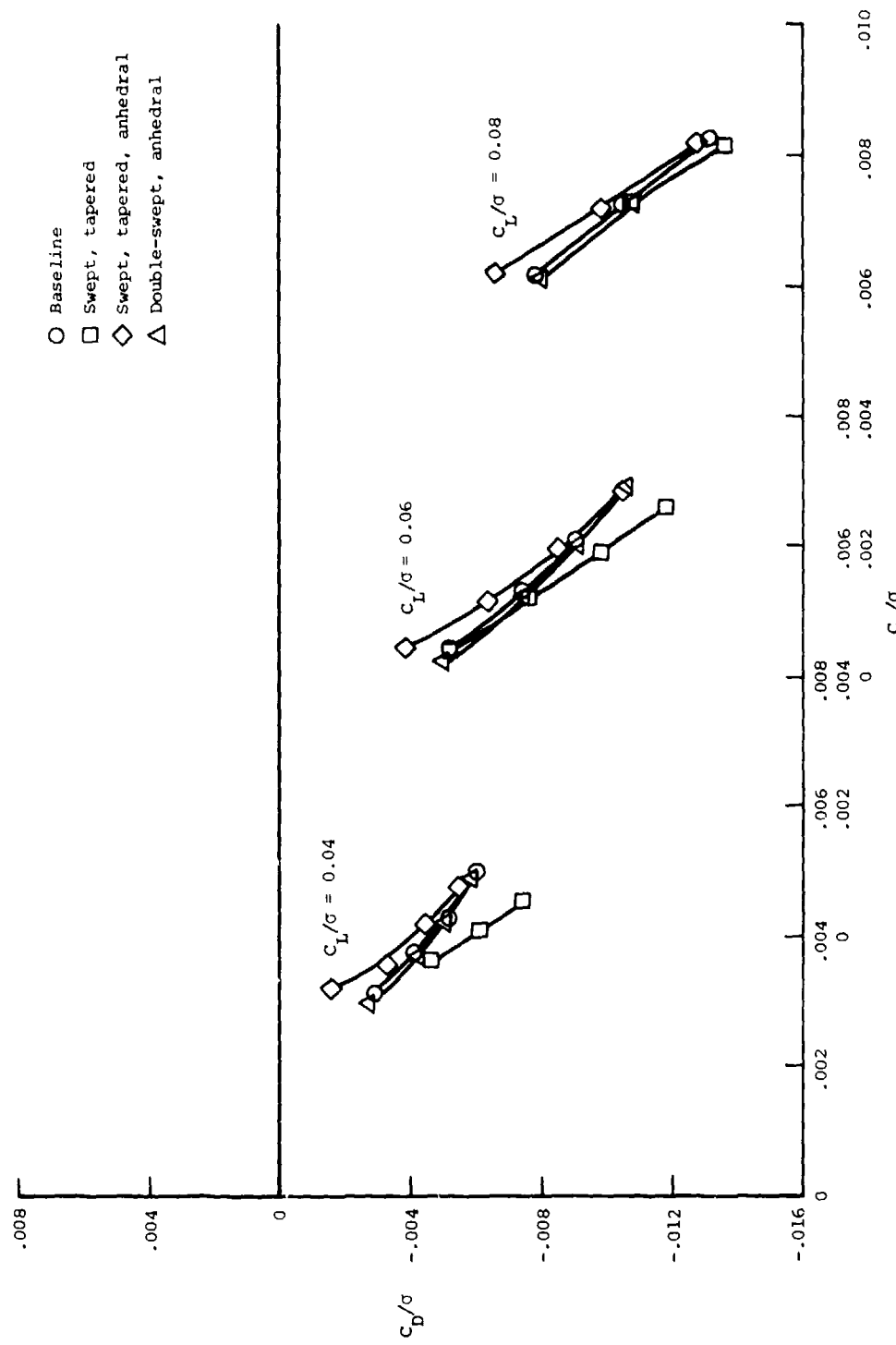
(c) $\mu = 0.35$.

Figure 11.— Concluded.
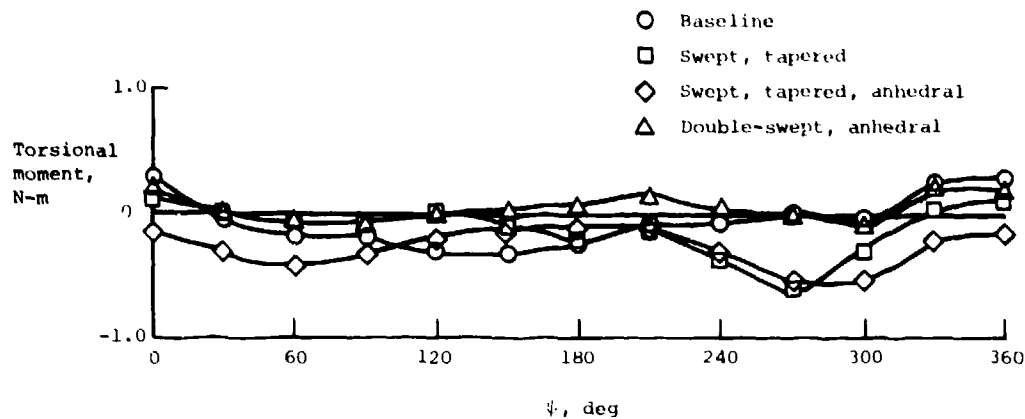
(a) $\mu = 0.20$; $C_L/\sigma = 0.08$; $\alpha_s = -4°$.
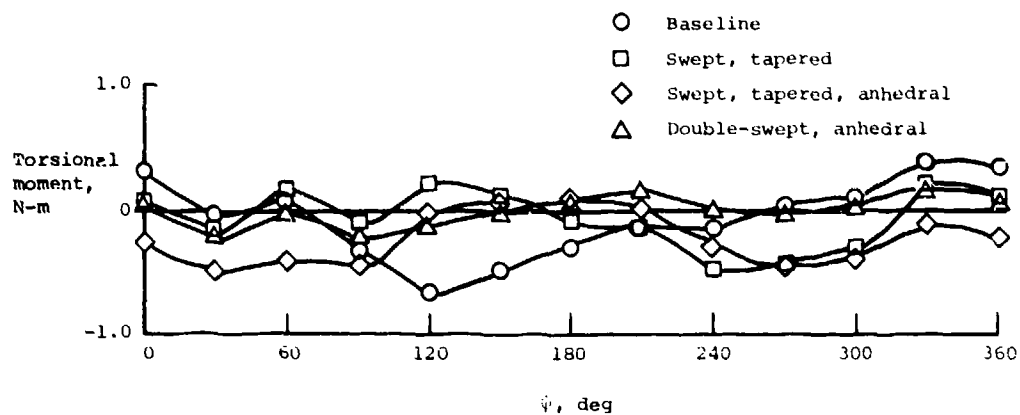
(b) $\mu = 0.30$; $C_L/\sigma = 0.08$; $\alpha_s = -4°$.
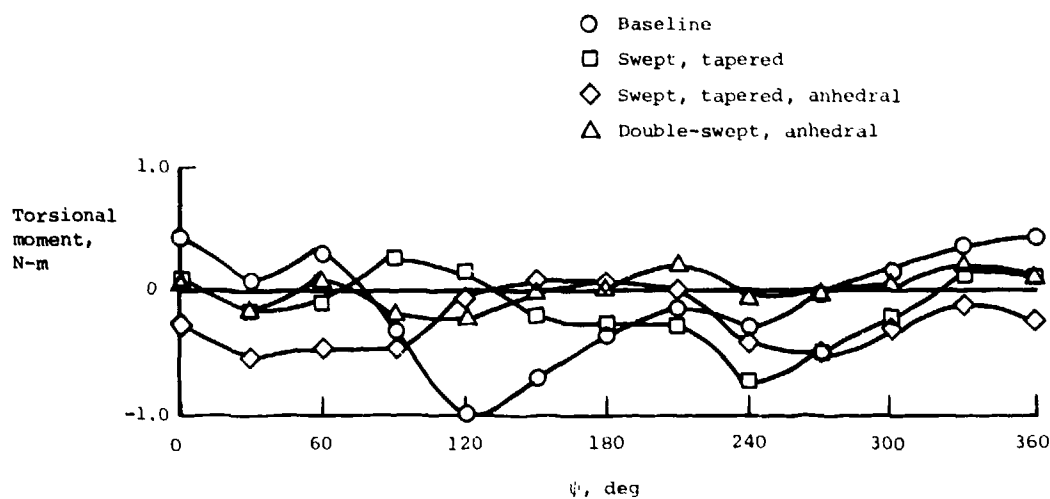
(c) $\mu = 0.35$; $C_L/\sigma = 0.08$; $\alpha_s = -6°$.

Figure 12.- Torsional moment at $r/R = 0.81$ (azimuthal distribution).
Positive nose-up.
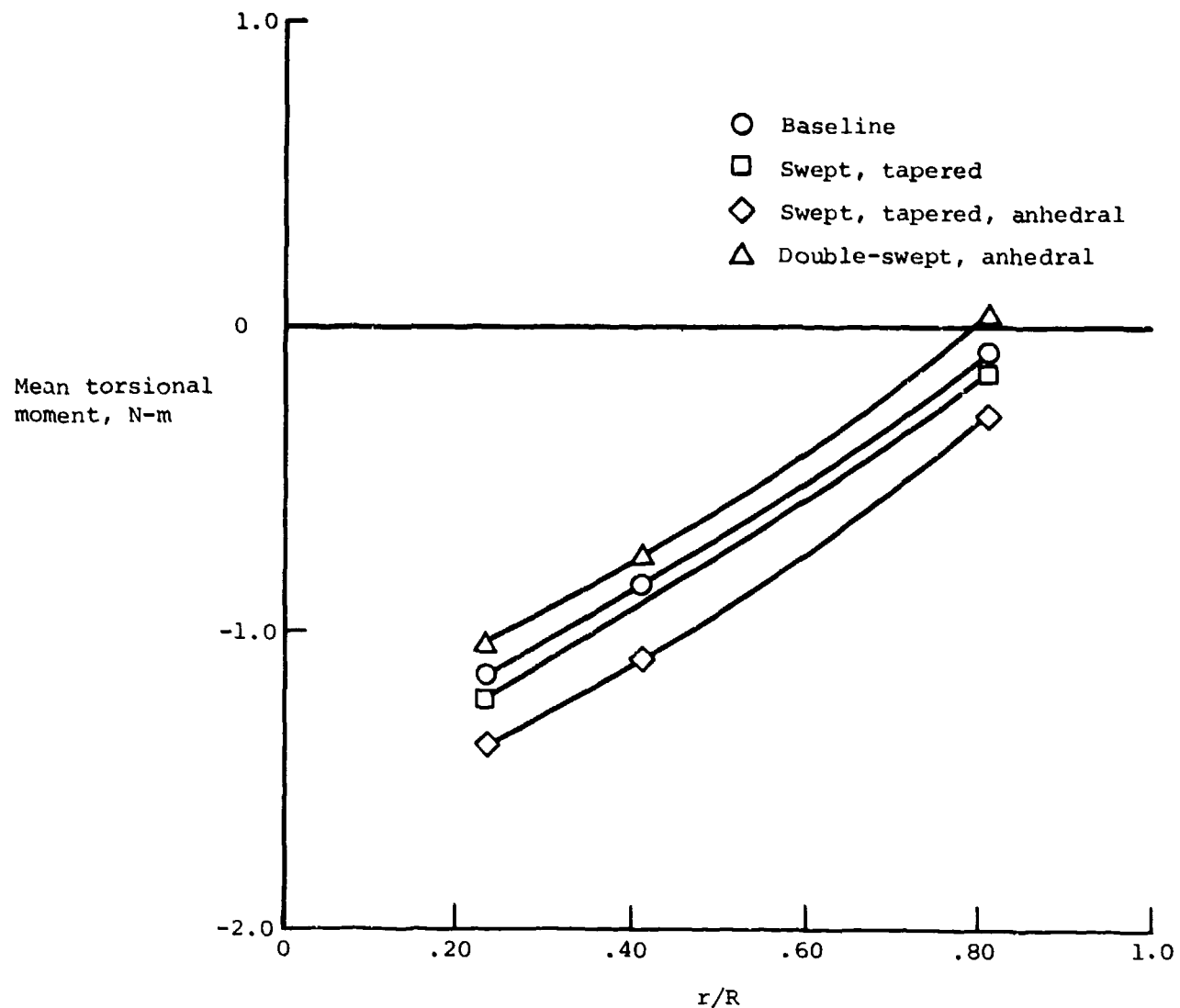
(a) $\mu = 0.20$; $C_L/\sigma = 0.08$; $\alpha_s = -4°$.

Figure 13.- Mean torsional moment (spanwise distribution).   Positive nose-up.

Legend:
○ Baseline
□ Swept, tapered
◇ Swept, tapered, anhedral
△ Double-swept, anhedral
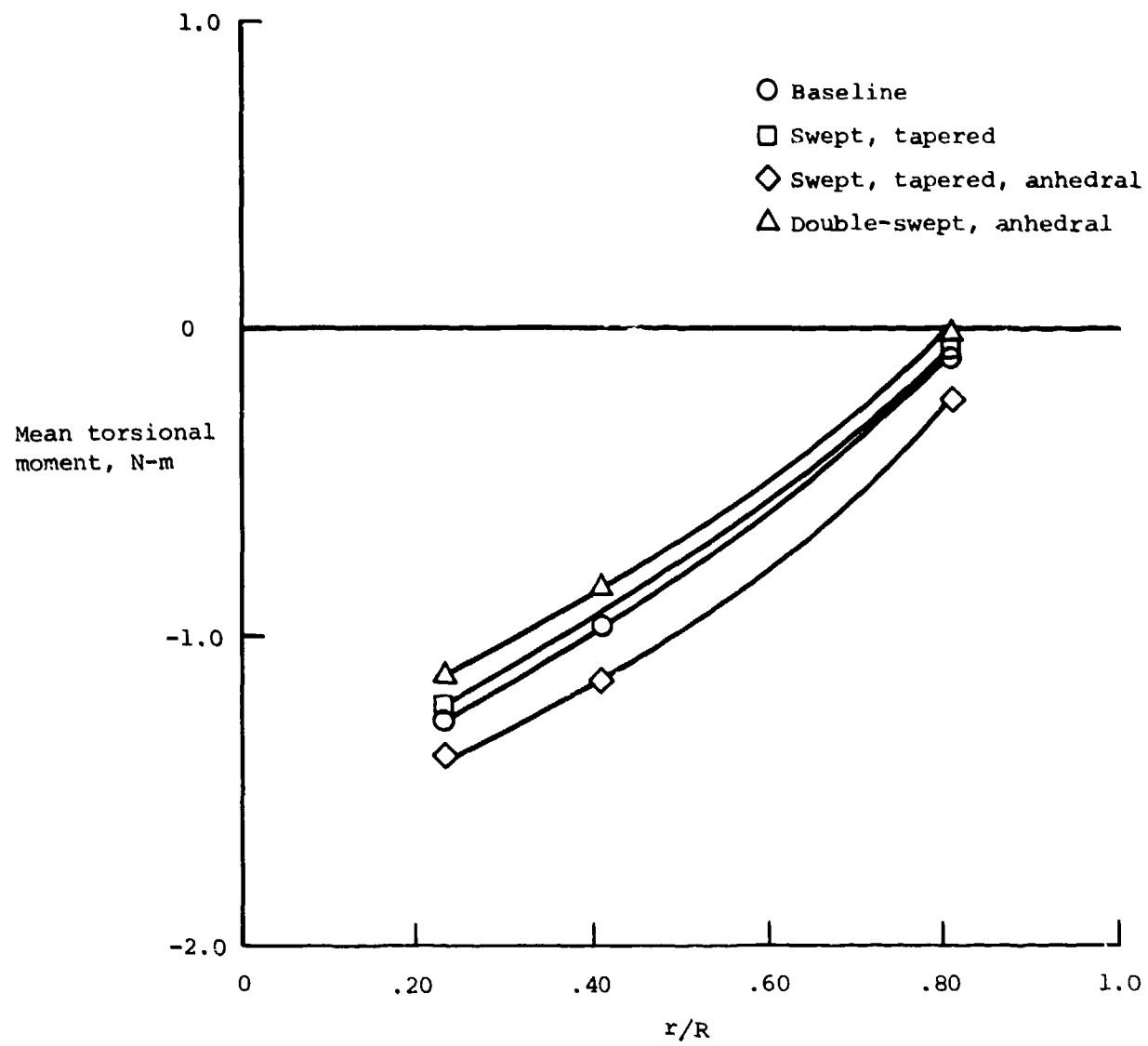
(b) $\mu = 0.30$; $C_L/\sigma = 0.08$; $\alpha_s = -4°$.

Figure 13.- Continued.

(c) $\mu = 0.35;$ $C_L/\sigma = 0.08;$ $\alpha_s = -6°.$
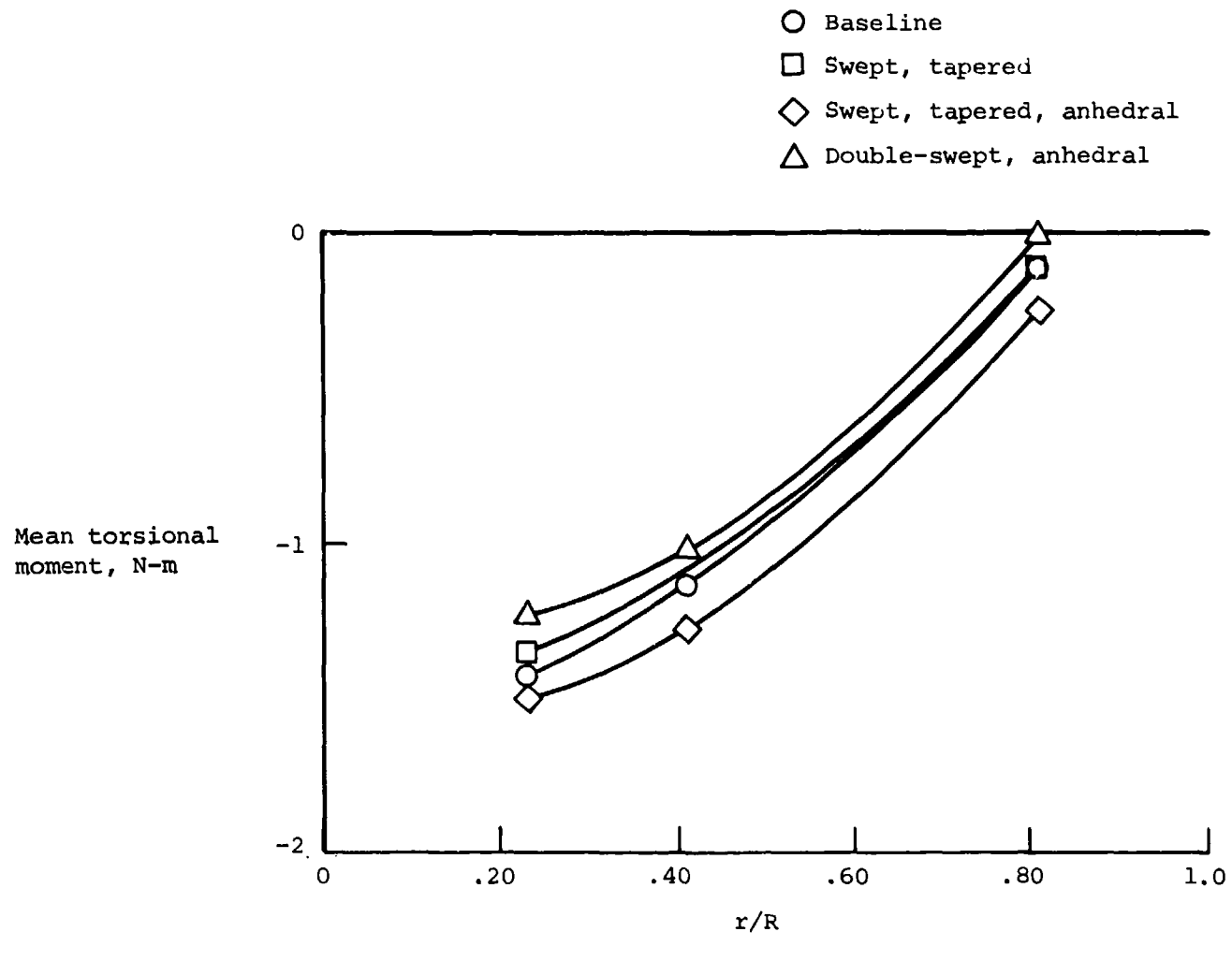
Figure 13.- Concluded.
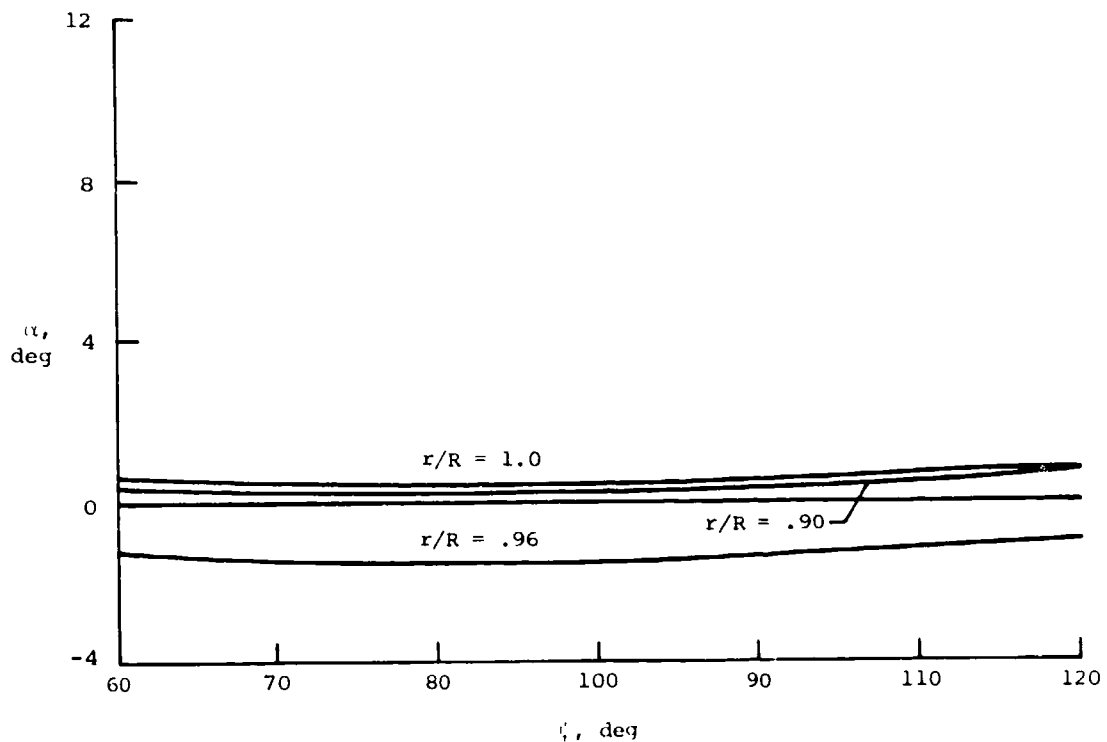
(a) $\mu = 0.20$; $C_L/\sigma = 0.08$; $\alpha_s = -4°$; uniform inflow.
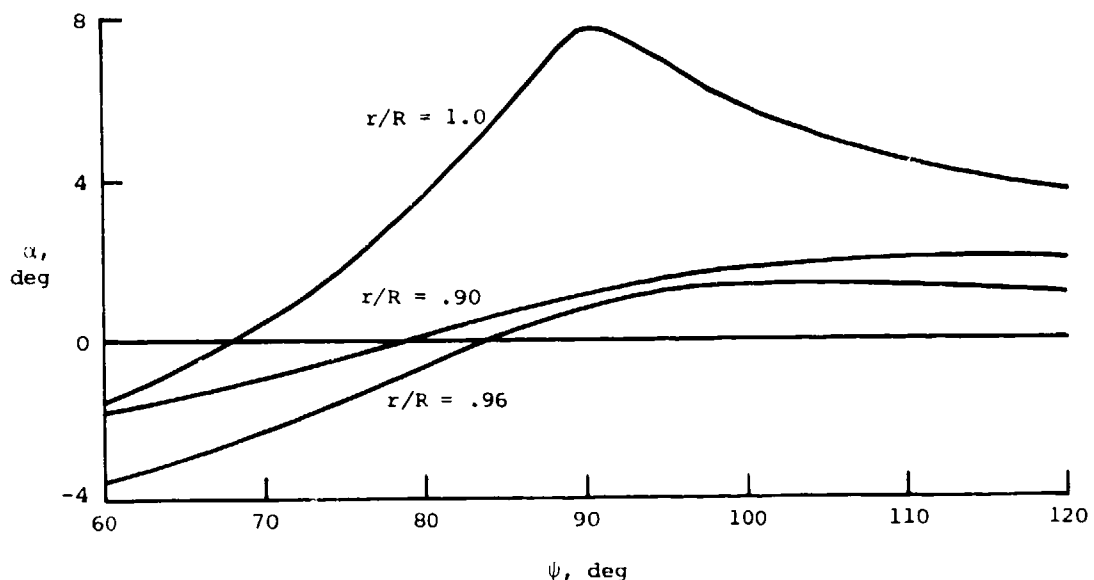
(b) $\mu = 0.20$; $C_L/\sigma = 0.08$; $\alpha_s = -4°$; nonuniform inflow.

Figure 14.- Calculated angle of attack on advancing side for baseline tip.
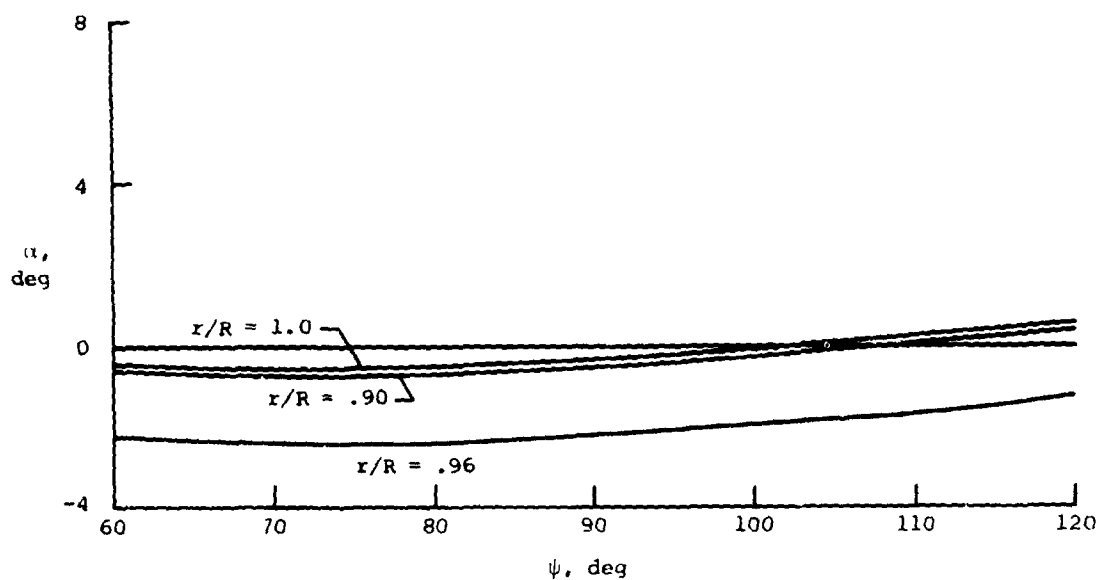
(c) $\mu = 0.30;$ $C_L/\sigma = 0.08;$ $\alpha_s = -4°;$ uniform inflow.
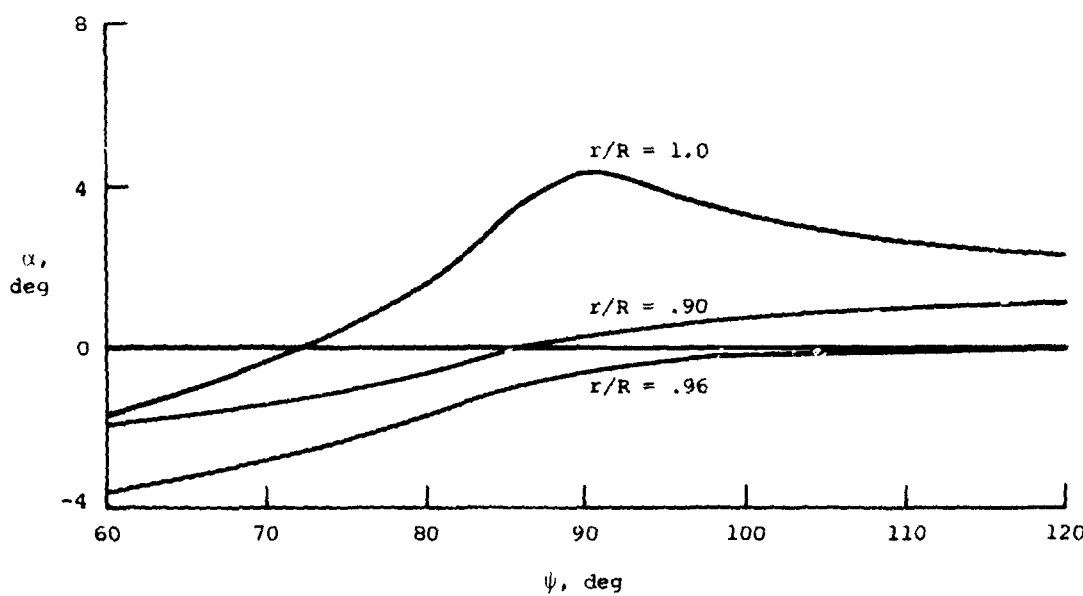
(d) $\mu = 0.30;$ $C_L/\sigma = 0.08;$ $\alpha_s = -4°;$ nonuniform inflow.

Figure 14.- Continued.
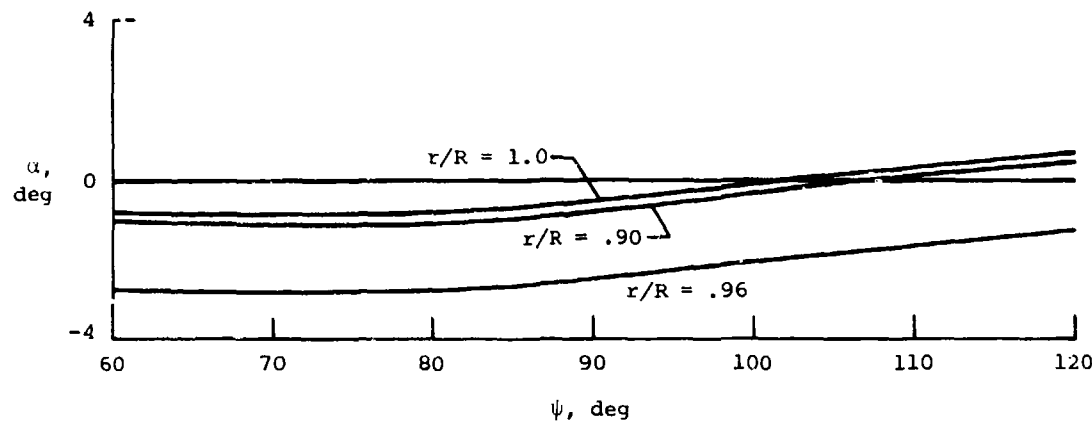
(e) $\mu = 0.35$; $C_L/\sigma = 0.08$; $\alpha_s = -6°$; uniform inflow.
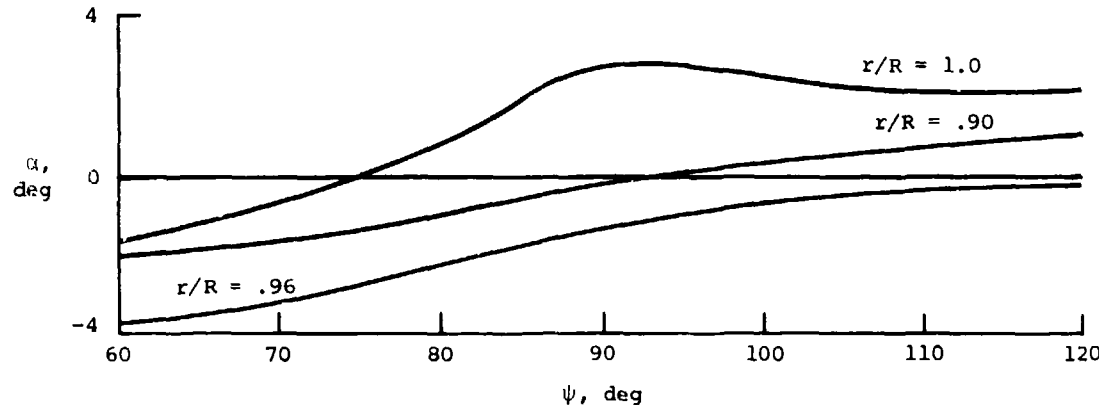
(f) $\mu = 0.35$; $C_L/\sigma = 0.08$; $\alpha_s = -6°$; nonuniform inflow.

Figure 14.- Concluded.
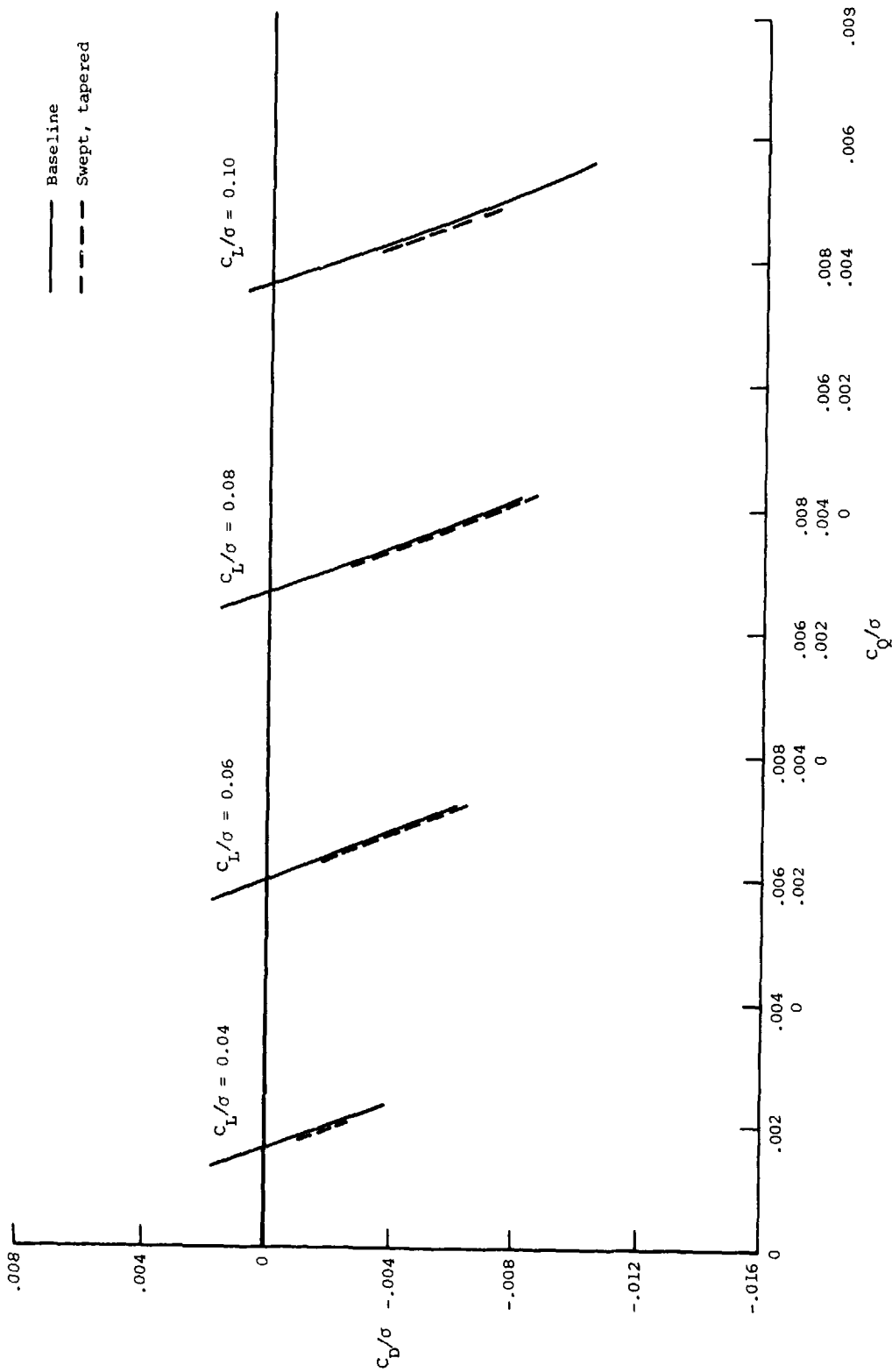
(a) $\mu = 0.20$; uniform inflow.

Figure 15.- Calculated rotor performance.
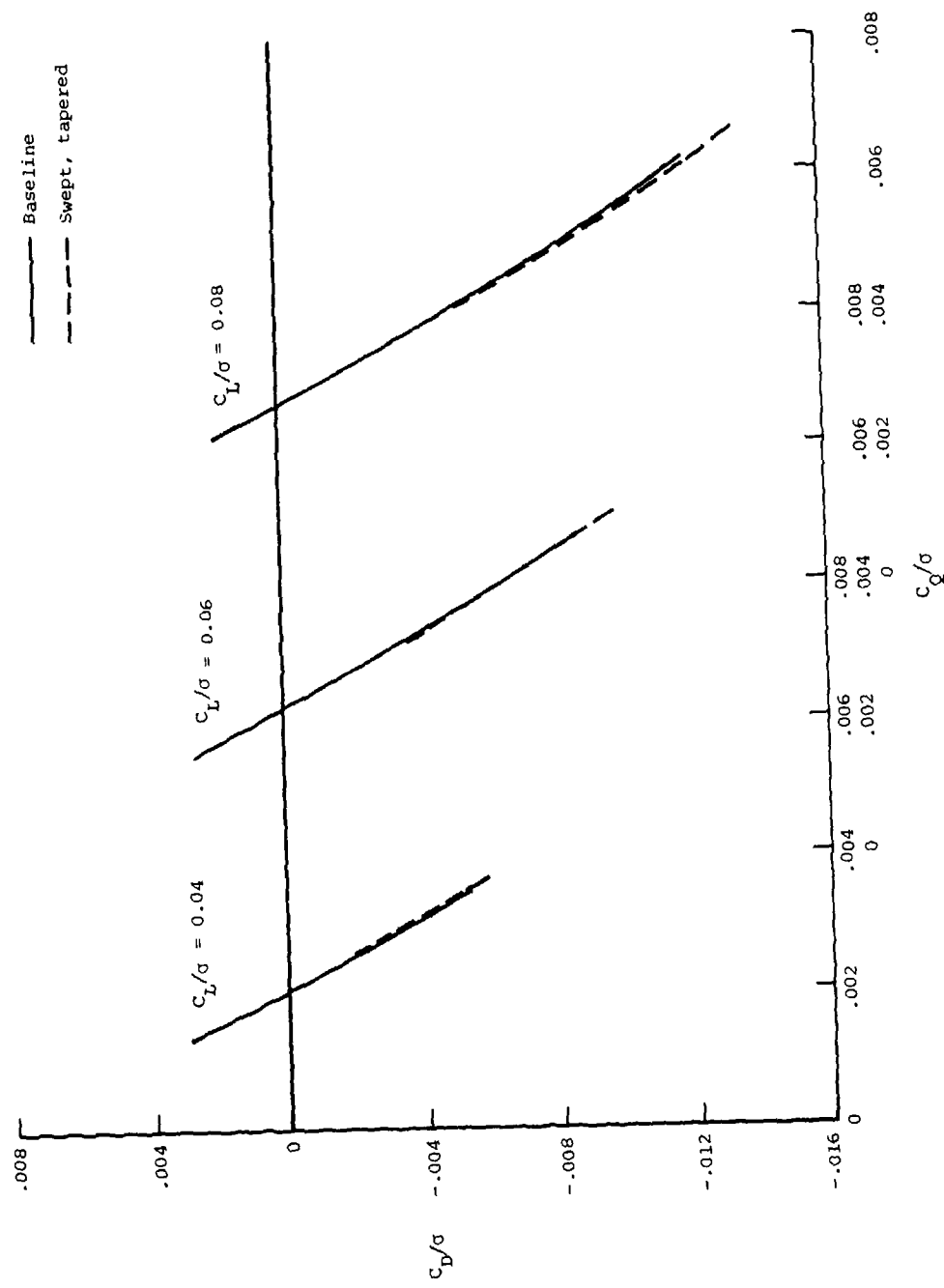
(b) $\mu = 0.30$; uniform inflow.

Figure 15.- Continued.

57
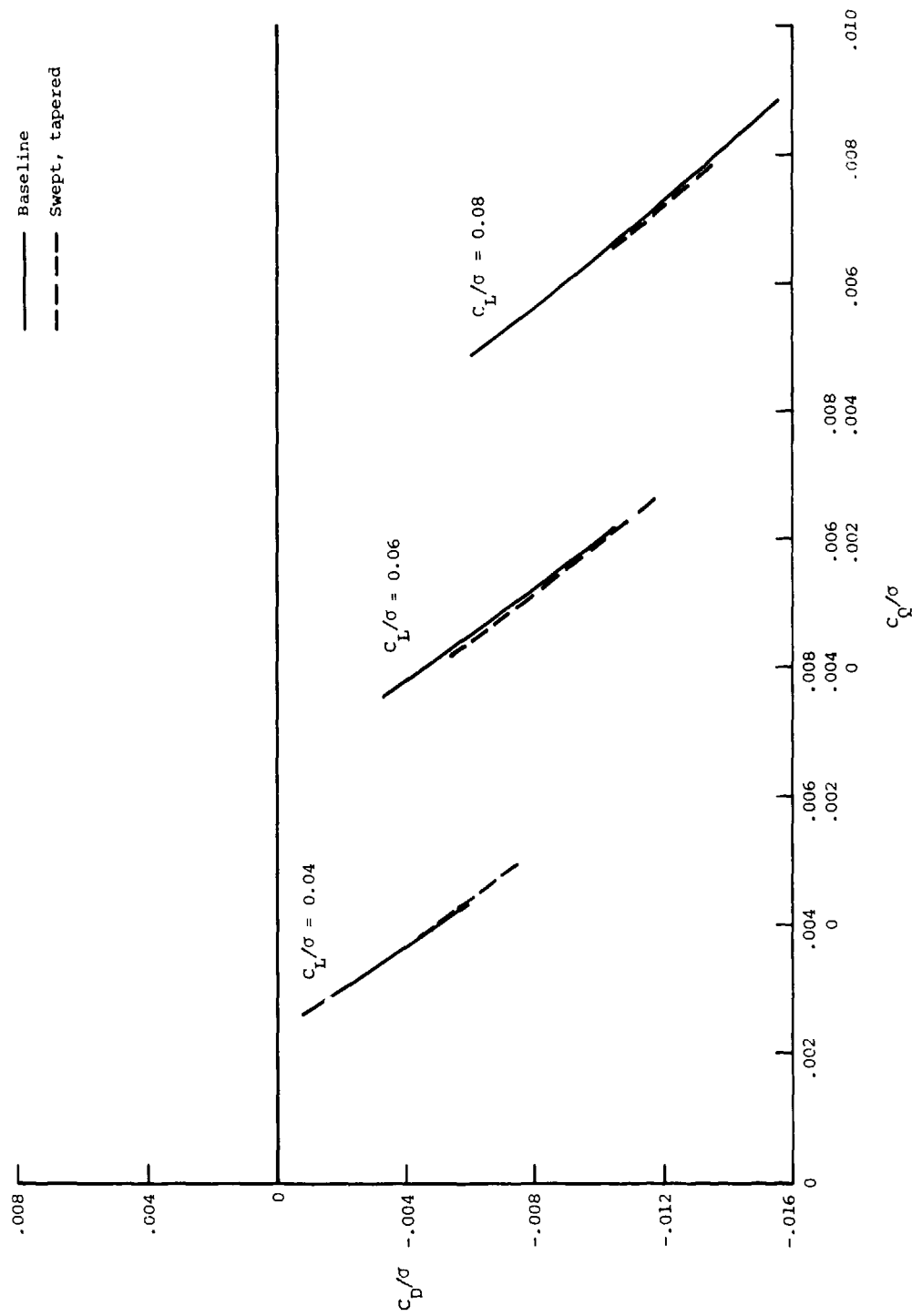
(c) $\mu = 0.35$; uniform inflow.

Figure 15.– Continued.
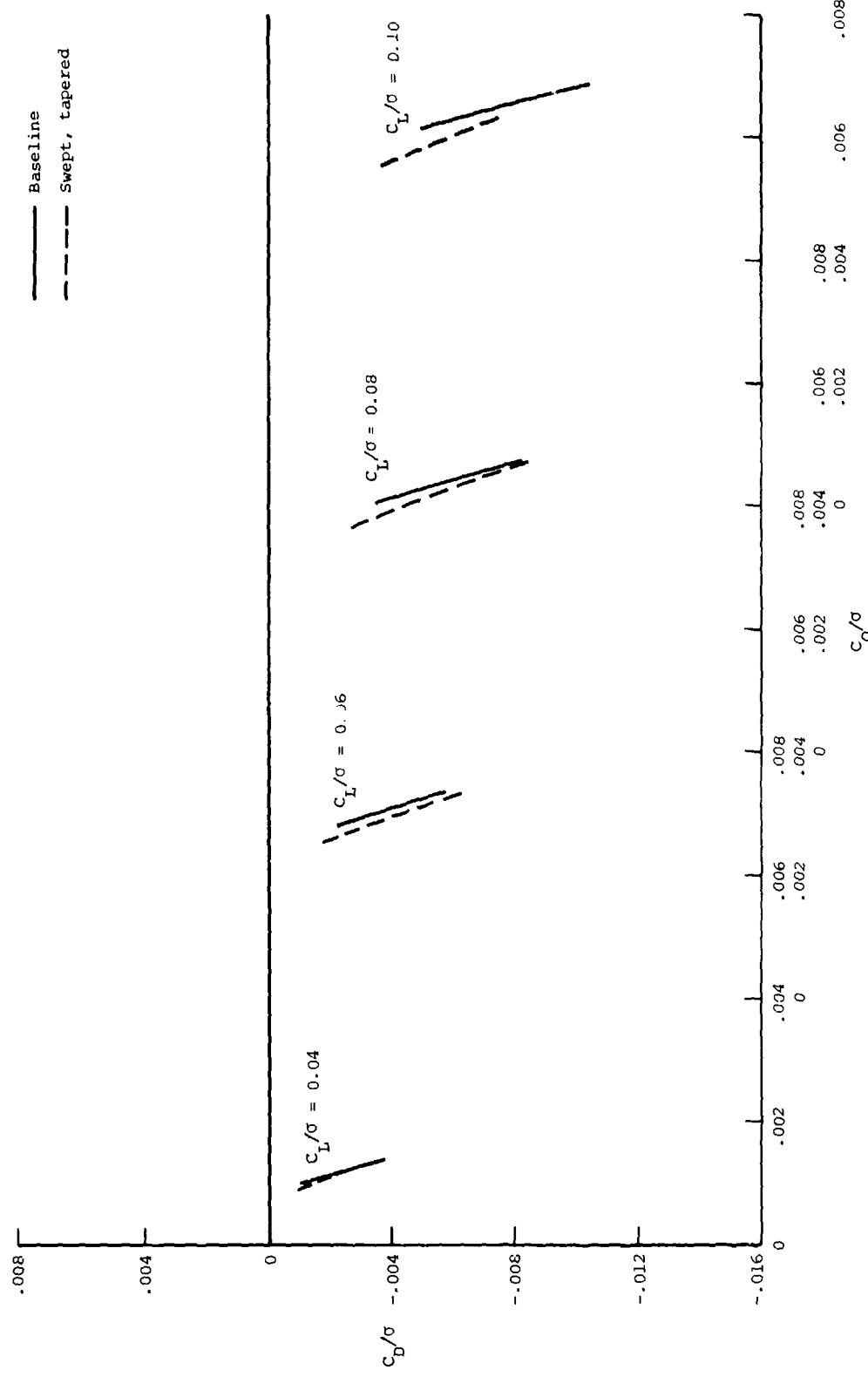
(d) $\mu = 0.20$; nonuniform inflow.

Figure 15.- Continued.
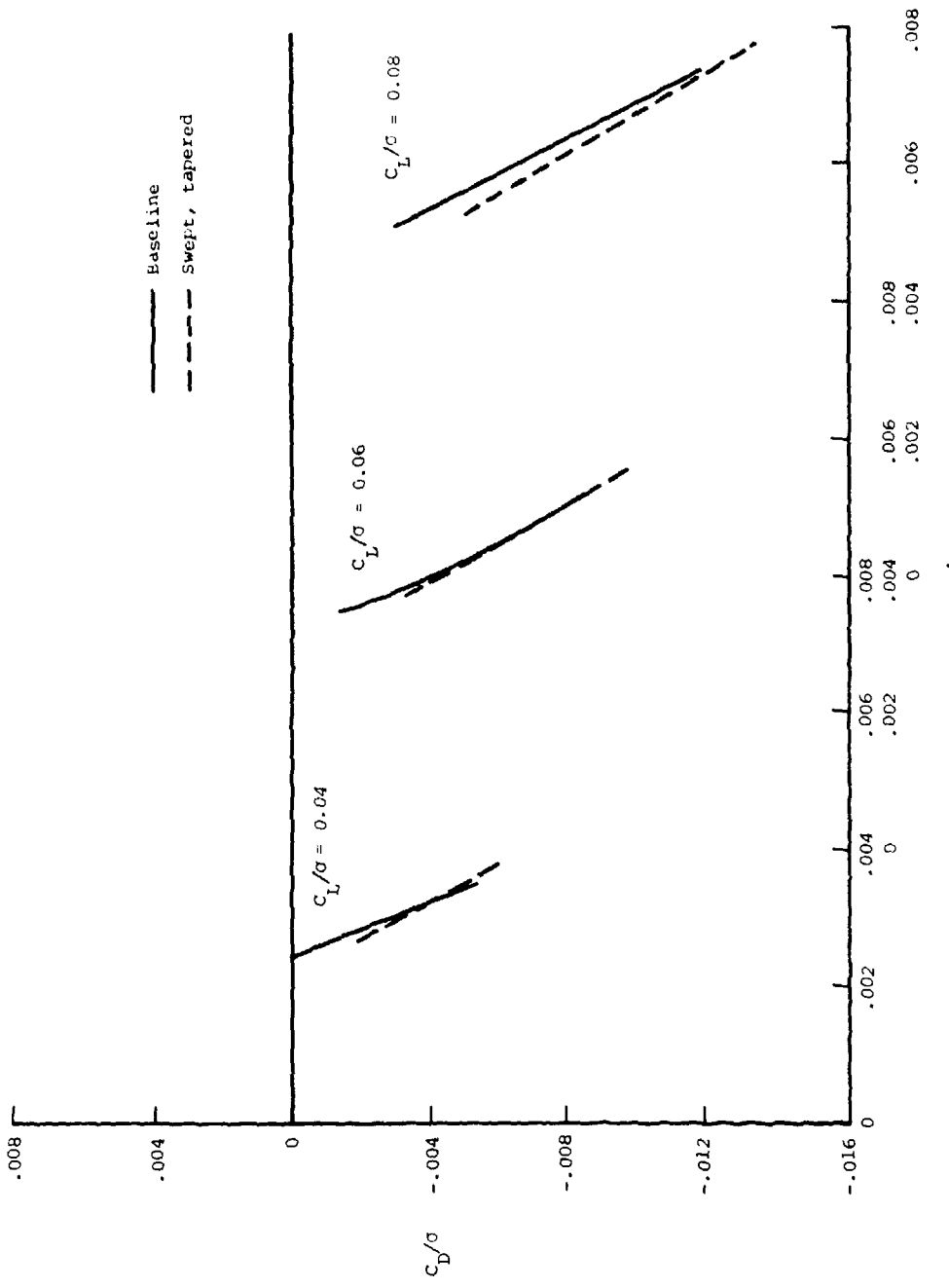
(e) μ = 0.30; nonuniform inflow.

Figure 15.- Continued.
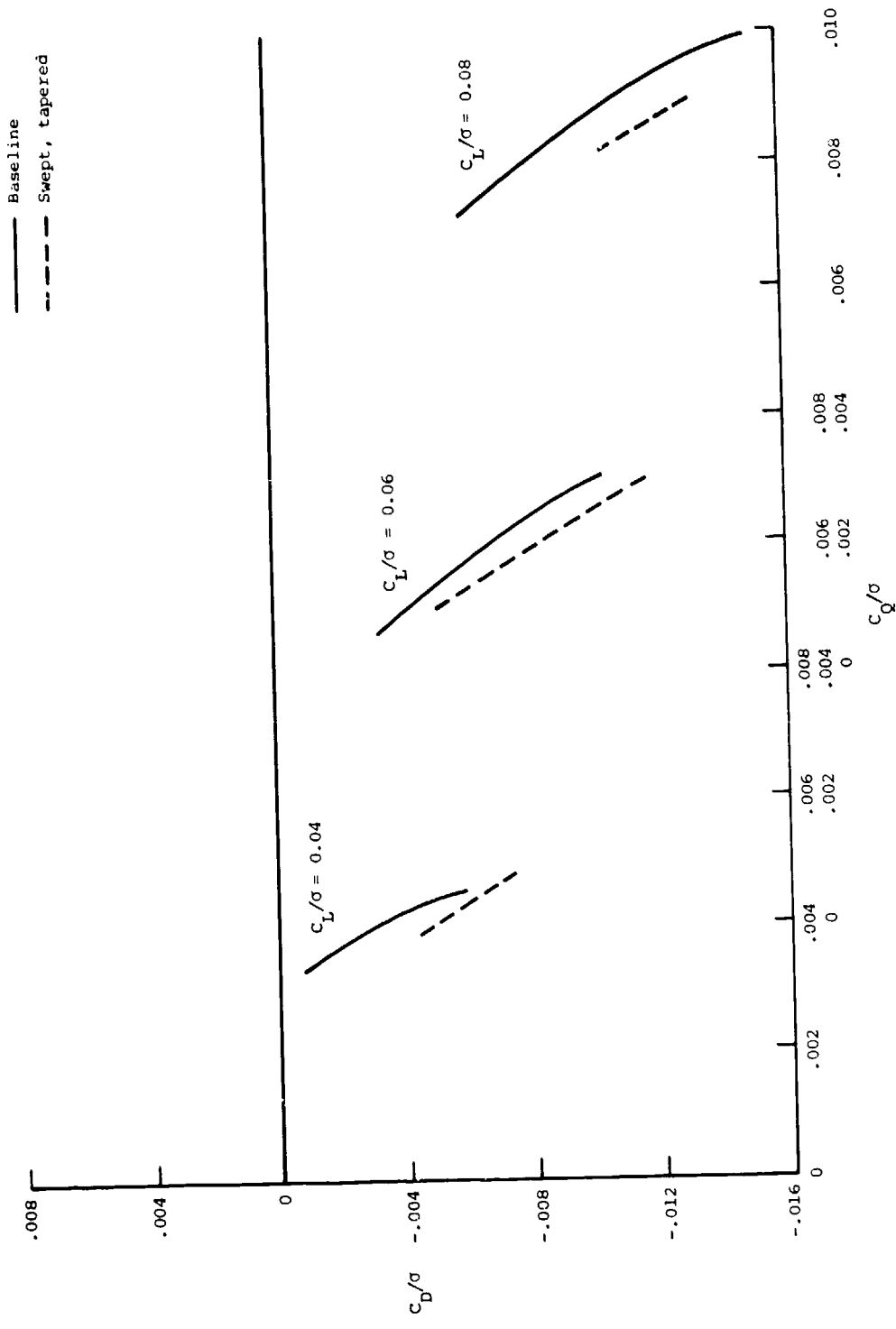
(f) $\mu = 0.35$; nonuniform inflow.

Figure 15.- Concluded.

1. Report No. NASA TP-1926 AVRADCOM TR 81-B-5	2. Government Accession No.	3. Recipient's Catalog No.
4. Title and Subtitle WIND-TUNNEL INVESTIGATION OF THE EFFECTS OF BLADE TIP GEOMETRY ON THE INTERACTION OF TORSIONAL LOADS AND PERFORMANCE FOR AN ARTICULATED HELICOPTER ROTOR		5. Report Date December 1981
		6. Performing Organization Code 505-42-13-04
7. Author(s) William T. Yeager, Jr., and Wayne R. Mantay		8. Performing Organization Report No. L-14674
9. Performing Organization Name and Address Structures Laboratory AVRADCOM Research and Technology Laboratories NASA Langley Research Center Hampton, VA 23665		10. Work Unit No.
		11. Contract or Grant No.
		13. Type of Report and Period Covered Technical Paper
12. Sponsoring Agency Name and Address National Aeronautics and Space Administration Washington, DC 20546 and U.S. Army Aviation Research and Development Command St. Louis, MO 63166		
		14. Army Project No. 1L262209AH76

16. Abstract

An investigation was conducted in the Langley Transonic Dynamics Tunnel to determine the effects of rotor blade tip geometry on the interaction between torsional loads and performance for an articulated helicopter rotor. Tests were conducted using four tip geometries at advance ratios of 0.20, 0.30, and 0.35. Geometric variations between tips consisted of taper, sweep, and anhedral.

17. Key Words (Suggested by Author(s)) Helicopters Articulated rotors Helicopter rotor Model rotor testing performance Blade tip geometry Torsional loads	18. Distribution Statement Unclassified - Unlimited Subject Category 02
19. Security Classif. (of this report) Unclassified	20. Security Classif. (of this page) Unclassified	21. No. of Pages 62	22. Price* A04